This is the author's version (accepted manuscript) of the work that was accepted for publication in AIAA Journal
The Version of Record is available online at https://doi.org/10.2514/1.J061143

Uncertainty Quantification for Aircraft Noise Emission Simulation: Methods and Limitations

Ulrich Römer*
Technische Universität Braunschweig, Schleinitzstr. 20, 38106 Braunschweig, Germany

Lothar Bertsch†
German Aerospace Center (DLR), Bunsenstr. 10, 37073 Göttingen, Germany

Sameer B. Mulani‡
The University of Alabama (UA), 1103E Bevill Building, Tuscaloosa, AL 35487, USA

Beat Schäffer§
Eidgenössische Materialprüfungs- und Forschungsanstalt (Empa), Überlandstr. 129, CH-8600 Dübendorf, Switzerland

Implementing measures for the reduction of aircraft noise impact, such as optimization of flight paths and aircraft, requires sophisticated simulation capabilities. These tools have to incorporate simulation of aircraft noise generation at the source, i.e., emission, and account for prevailing sound propagation effects in order to ultimately predict the noise levels as received on the ground. Obviously, understanding the associated uncertainties is crucial when aiming at a reliable and meaningful assessment. It also becomes essential if comparing different technologies, mixing experimental and numerical data, or using simulation methods of different fidelity, e.g., semi-empirical and first-order methods. This research focuses on quantifying uncertainties in the first step in aircraft noise simulation, i.e., the prediction of the emission situation. The quantified uncertainties reflect imperfections of models for different aircraft noise sources and variability of model input parameters at different operating conditions. We present a general framework, which also accounts for limited knowledge of the underlying data distributions, and we provide quantitative comparisons of different uncertainty methods. In particular, we compare the first-order second-moment analysis to higher-order Polynomial Chaos methods and discuss the advantages and disadvantages of the different methods.

Nomenclature

FOSM	First-Order Second-Moment Method
PANAM	Parametric Aircraft Noise Analysis Module

*corresponding author, Junior professor, Department of Mechanical Engineering
†Senior Scientist, Institute of Aerodynamics and Flow Technology
‡Associate Professor, Department of Aerospace Engineering and Mechanics
§Senior Scientist, Laboratory for Acoustics / Noise Control

LHS	Latin Hypercube Sampling
HO	Higher-Order
MC	Monte Carlo
PC	Polynomial Chaos
PLE	Polynomial Chaos Expansion
RSS	Rotor Stator Spacing, [-]
TAS	True Air Speed
N1	Revolutions Per Minute
UQ	Uncertainty Quantification
CDF	Cumulative Distribution Function
PDF	Probability Density Function

Metrics

$L_{\mathrm{em},\alpha}$	sound pressure level of source α emission, dB
$L_{\mathrm{em},t}$	sound pressure level of the total vehicle emission, dB

Terminology

Φ	angle for azimuthal / lateral directivity, +90° equals to starboard
Θ	angle for polar / longitudinal directivity, 0° equals flight direction
μ	mean value
σ	standard deviation

Indices

t.e.	sum of trailing edge noise (wing, all sources)
l.e.	sum of leading edge noise (wing, all sources)
gear	sum of main and nose landing gear noise
fan	sum of inlet and exhaust fan noise (all engines)
jet	sum of jet noise (all engines)

I. Introduction

Uncertainties are ubiquitous in physical systems. In the past, scientists and engineers have been developing mathematical techniques to represent complex physical phenomena without accounting for uncertainties. Hence, the results provided by such techniques do not precisely match or predict the experimental observations of real data due

to unaccounted uncertainties. These uncertainties may originate from the inherent variability of the input parameters (aleatoric uncertainties) and limited knowledge about the parameters and assumptions made while developing the mathematical models to predict noise (epistemic uncertainties) [1]. The confidence in mathematical models can be improved by the inclusion of uncertainties of the modeling. This is known as uncertainty quantification (UQ), a field that has attracted much attention recently. In UQ, the variation of the response due to the presence of uncertainties is studied in [2, 3], referred to as forward problem or uncertainty propagation. UQ for high-dimensional systems with expensive functions becomes computationally exhaustive, especially with multi-physics problems, e.g., aircraft design and space vehicle design. Therefore, there is a need to develop algorithms that yield highly accurate stochastic response models with minimal computational costs. Among the techniques employed for UQ are Monte Carlo simulation (MC) [4], perturbation approaches [5], Neumann expansions [6], weighted integral methods [7], first-order second-moment methods (FOSM), first and second-order reliability methods [8], and spectral stochastic finite element methods [2]. Amongst the latter methods, spectral expansion techniques such as Polynomial Chaos expansions (PCE) [2] have become increasingly popular in recent decades due to their mathematical elegance, mean square convergence, and ability to handle random inputs with strong variation [9–11]. The numerous benefits of PC over other methods for UQ have led to applications in many disciplines, such as structural analysis [2], fluid dynamics [12, 13], composite structures [14], and stability and control [15].

In the same way, simulation models for predicting exterior aircraft noise have been much improved over the last decades. Two recent studies demonstrated the potential of these simulations and their applicability for existing aircraft [16] and novel vehicle concepts [17]. Yet, uncertainty assessments are still scarce, despite their importance in the field. A possible approach for evaluating uncertainties for a parametric aircraft noise simulation has been presented in [18]. The overall goal of the latter study was to estimate the uncertainty of both noise emission and ground exposure levels under arbitrary operating conditions for different aircraft designs and technologies. The chosen approach was FOSM, which had been previously applied to the best practice aircraft noise calculation program FLULA2 in [19] and [20]. However, the FOSM approach relies on small input parameter uncertainties, and a validation of its applicability in an aircraft noise prediction context remains open. The objective of the current study is to compare the FOSM with two other widely used UQ methods, namely, the MC and PC, at the example of specific aircraft noise emission test cases. We focus on emission simulations only, as a first step towards handling the entire noise prediction process. The aim of the comparison is to show similarities and differences of the different UQ methods, their advantages, and disadvantages and to establish application limits, with a focus on aircraft noise simulations. Hereby, the study aims to include different types of uncertainties, i.e., uncertainties accounting for noise modeling simplifications and parametric input uncertainties, which complicates the UQ study since many parameters need to be taken into account. Furthermore, this paper addresses the limited availability of information on data and the consequences on the quantified uncertainties. Indeed, parametric studies with complex models, which integrate different disciplinary sub-modules, frequently suffer

from limited data on input and model uncertainties. Scarce data can be modeled with imprecise probabilities, and we propose to use a p-box approach to model both missing correlations and distribution information. These modeling aspects, together with the aforementioned comparisons, introduce new elements into the UQ aircraft noise literature.

The paper is structured as follows. Section II gives an overview of the aircraft system noise prediction method used in this study and introduces the test cases used for the methods comparison for the noise emission. Section III describes the different UQ methods, i.e., FOSM, Monte Carlo, and Polynomial Chaos. Section IV reports the results of the application of the methods to the test cases and their comparisons. The discussion of the results and an outlook to possible future research are given in Section V. Finally, the conclusions are given in Section VI.

II. System Noise Prediction Modeling Approach

Aircraft system noise is defined according to [21] as *"the source noise emitted by an aircraft in flight, propagated through the atmosphere, and received by observers or sensors on the ground."*. For *scientific models*, as opposed to *best practice models* such as AzB [22, 23], FLULA2 [24], ECAC Doc.29 [23, 25], and Doc 9911 [26], the focus of system noise prediction lies on a component-wise and parametric prediction. A definition of this classification is provided in [27, 28]. These models use a so-called component-based approach to describe the aircraft as the aggregation of individual noise sources on board. In a time-stepping approach, the aircraft noise emission of each component is modeled along a discretized flight trajectory, where the current aircraft operating conditions are taken into account at each time step t, along the trajectory. Energetic summation of all assessed incoherent noise sources yields the total vehicle noise emission $L_{\mathrm{em},t}$ for time step t.

For the individual components α, emission levels are predicted with a defined parametric noise source model $\mathcal{M}_\alpha$. These models are parametric with respect to a source specific vector of input parameters $\boldsymbol{x}_{\alpha;\mathrm{inp}}$, describing not only the airframe and the engine geometry, but also the operating condition of the entire aircraft, e.g., engine thrust setting and deflection angles of high-lift elements. The inflow velocity is one parameter that will directly affect all airframe noise sources. We also collect all parameters, which specify the model and simulation and which are not subject to uncertainty in a vector $\boldsymbol{z}_{\alpha;\mathrm{inp}}$. Examples are the polar and lateral emission angles Θ and Φ. Hence, the predicted levels for each source α depend on the input parameters as

$$y_\alpha = \mathcal{M}_\alpha(\boldsymbol{x}_{\alpha;\mathrm{inp}}, \boldsymbol{z}_{\alpha;\mathrm{inp}}), \tag{1}$$

where $y_\alpha = L_{\mathrm{em},\alpha}$ denotes the model output quantity for each component.

Several *scientific* models, namely NASA's ANoPP 2 [29], ONERA's CARMEN [30] and DLR's PANAM [31] tool, are currently under development. A comparison of these methods is given in [16] and [17]. In the present study, the DLR noise prediction tool PANAM is used. Consistent with previous work [18], this study focuses on the major noise

source models, namely, a trailing edge (t.e.), leading edge (l.e.), landing gear (gear), engine fan (fan), and engine jet (jet) model, hence, $\alpha \in \{\text{t.e.}, \text{l.e.}, \text{gear}, \text{fan}, \text{jet}\}$. These models contribute to the total aircraft noise emission $L_{\text{em},t}$ by energetic summation as

$$L_{\text{em},t} = 10 \cdot \log_{10}\left(\sum_{\alpha} 10^{L_{\text{em},\alpha}/10}\right), \tag{2}$$

where both $L_{\text{em},t}$ and $L_{\text{em},\alpha}$ depend on the fixed parameters, such as the polar and lateral emission angles Θ and Φ. Additionally, the partial emissions $L_{\text{em},\alpha}$ depend on a component-specific vector of uncertain input parameters as described above. Hence, the total emission level $L_{\text{em},t}$ depends on the collection of all individual component input parameters, which is not explicitly indicated for simplicity. The models, as well as their input parameters, which are used to predict the noise contribution of each source α, are listed in Table 1. Based on the input data $\boldsymbol{x}_{\alpha;\text{inp}}$, each model predicts a corresponding emission spectrum, which changes depending on the direction toward predefined ground observers. Typical emission spectra of a conventional mid-range transport aircraft during a realistic approach and

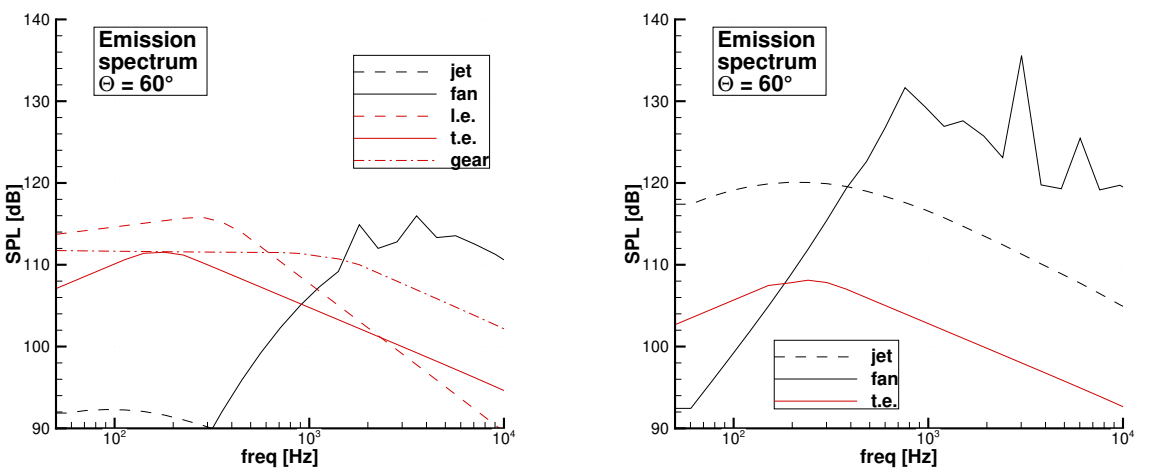

(a) Approach situation: 60° emission spectrum in ref. distance of 1 m (b) Departure situation: 60° emission spectrum in ref. distance of 1 m

Fig. 1 Application case: Selected emission situations of a mid-range transport aircraft along approach and departure.

departure procedure are exemplary shown in Figs. 1(a) and 1(b). Note that this example will be used later in this study for the numerical experiments and comparisons in Section IV. For the approach situation, the influence of airframe and engine components is of similar magnitude, whereas the selected departure situation is dominated by fan noise. The exemplary noise emission spectra are depicted for a preselected polar emission angle of $\Theta = 60°$ in the aircraft symmetry plane ($\Phi = 0°$) and at a reference distance of 1 m. Superimposing the contributions of the individual sources will finally yield the total sound pressure level $L_{\text{em},t}$ for the entire aircraft under the selected operating condition and emission angles. The selected emission situations are comprised of two typical operating condition with very different

Table 1 Source models with modeling standard uncertainty $\sigma_{\alpha;\mathbf{mod}}$ and selected input parameters $\boldsymbol{x}_{\alpha;\mathbf{inp}}$.

Source model M_α [Refs.]	**Standard deviation** $\sigma_{\alpha;\mathrm{mod}}$	**Input parameters** $\boldsymbol{x}_{\alpha;\mathrm{inp}}$
Trailing edge, $L_{\mathrm{em,t.e.}}$ [32–37]	±1 dB	TAS ($x_{\mathrm{af};1}$), t.e. sweep angle ($x_{\mathrm{af};2}$), wing loading ($x_{\mathrm{af};4}$)
Leading edge, $L_{\mathrm{em,l.e.}}$ [32–35]	±1 dB	TAS ($x_{\mathrm{af};1}$), l.e. sweep angle ($x_{\mathrm{af};3}$), wing loading ($x_{\mathrm{af};4}$)
Landing gear, $L_{\mathrm{em,gear}}$ [32–35]	±1 dB	TAS ($x_{\mathrm{af};1}$), wing loading ($x_{\mathrm{af};4}$)
Fan, $L_{\mathrm{em,fan}}$ (incl. acoustic lining) [38, 39]	±2 dB	N1 ($x_{\mathrm{fan};1}$), RSS ($x_{\mathrm{fan};2}$), total mass flow ($x_{\mathrm{fan};3}$), relative tip Mach ($x_{\mathrm{fan};4}$)
Jet, $L_{\mathrm{em,jet}}$ [40]	±1.5 dB	core exhaust velocity ($x_{\mathrm{jet};1}$), bypass exhaust velocity ($x_{\mathrm{jet};2}$), TAS ($x_{\mathrm{jet};3}$; equal to $x_{\mathrm{af};1}$), total jet core exhaust temp. ($x_{\mathrm{jet};4}$)

configurational settings as could be experienced along a realistic approach and departure flight.

In the example (Figs. 1(a) and 1(b)), the predicted deterministic approach overall sound pressure levels are:

- $L_{\mathrm{em,jet}}$ = 102.5 dB, $L_{\mathrm{em,fan}}$ = 123.0 dB, $L_{\mathrm{em,gear}}$ = 124.3 dB, $L_{\mathrm{em,l.e.}}$ = 125.8 dB, $L_{\mathrm{em,t.e.}}$ = 121.1 dB

These source contributions add up to a deterministic overall vehicle noise emission of $L_{\mathrm{em},t}$ = 129.9 dB. Predicted departure overall sound pressure levels are per noise:

- $L_{\mathrm{em,jet}}$ = 131.0 dB, $L_{\mathrm{em,fan}}$ = 138.8 dB, $L_{\mathrm{em,t.e.}}$ = 118.0 dB

Trailing edge and landing gear do not contribute since these devices are not deployed. All source contributions add up to a deterministic overall departure noise level of $L_{\mathrm{em},t}$ = 139.5 dB.

Different emission angles will result in different emission spectra according to the directivity of each noise source. If the overall goal is to assess the noise exposure on the ground (e.g., on a whole grid of receivers), all emission angles towards all predefined observer locations must be evaluated. In order to determine the overall system noise $L_{\mathrm{im},t}$ along a complete flight path, the emitted signal $L_{\mathrm{em},t}$ is propagated through the atmosphere, accounting for geometric spreading, atmospheric attenuation, possibly barrier effects due to terrain, and further "excess attenuation" effects, usually accounted for by for lateral attenuation. Propagation algorithms and lateral attenuation are described, e.g., in the standard ISO 9613 [41] and in the SAE AIR 1751 [42], respectively. The resulting noise exposure $L_{\mathrm{im},t}$ at multiple ground observers can then be visualized by noise isocontour maps, e.g., [18–20]. Note, however, that propagation modeling and associated uncertainties are not in the scope of this paper. Instead, the study is limited to the uncertainties of an approach and a departure simulation at the emission level associated with the noise prediction of $L_{\mathrm{em},t}$ under a fixed emission angle.

III. Uncertainty Quantification

A. Overview

This section describes the different methods for UQ and how they can be used to address settings with fully and incompletely specified probability distributions. We introduce the stochastic models and review the UQ-aerospace literature. Here, for propagating parametric uncertainties, MC Simulation [4], FOSM [5], and non-intrusive PC with least squares [43] are used.

Some recent UQ aerospace applications are discussed in [44, 45]. Contributions focusing on PCE developments and applications are given in [46, 47]. A PCE with Kriging was applied in [48] to estimate uncertainties of airfoils and an engine nacelle and in [49] to benchmark problems with multi-fidelity modeling. Recent applications of epistemic UQ in aerospace systems are described in [50, 51]. UQ and global sensitivity analysis for aircraft with on-board fuel cells are discussed in [52], whereas the cabin noise prediction under uncertainty, has been treated in [53]. Another recent contribution considers external stochastic disturbances on flight mechanics and flight control with a multifidelity approach [54]. UQ of the system noise during take-off and landing of supersonic transport aircraft was carried out using the PCE and epistemic uncertainties in [55].

In this research, we account for the fact that a deterministic sound emission model is only an approximation of an actual physical sound generation process, in the sense that the model input parameters are not known exactly, and the model itself is a simplified description of reality. To account for uncertainty, we use random variables in the model. As opposed to equation (1), we use a capital bold letter, i.e., $\boldsymbol{X}_{\alpha;\mathrm{inp}}$, to denote the random input vector associated to source α, and drop the additional fixed parameters $\boldsymbol{z}_\alpha$ in the following, for simplicity. For each noise source α, we now consider the probabilistic model

$$Y_\alpha = \mathcal{M}_\alpha(\boldsymbol{X}_{\alpha;\mathrm{inp}}) + X_{\alpha;\mathrm{mod}}, \tag{3}$$

where in addition to the model input random variables, $X_{\alpha;\mathrm{mod}}$ is a variable accounting for uncertainties due to possible model simplifications, as described in [18]. The standard deviations are provided in Table 1 for each source model M_α. Such an additive model error correction is widespread in the statistics community [56]. As before, the individual emission levels can be combined into the total emission level as stated in Eq. (2), which is recast here as

$$Y_t = 10 \cdot \log_{10}\left(\sum_\alpha 10^{Y_\alpha/10}\right), \tag{4}$$

where the total emission level Y_t is also a random variable now, which additionally depends on the model uncertainties $X_{\alpha;\mathrm{mod}}$.

For each random variable X_i (related to model errors $_{\mathrm{mod}}$ or model inputs $_{\mathrm{inp}}$), a specification of the probability density function ρ_{X_i} is needed. Moreover, correlations between random variables may exist and need to be taken into

account. In the first step, we assume that the distribution of the input variables $\rho_{\boldsymbol{X}}$ has been precisely inferred from data. To simplify the uncertainty treatment we further assume that $\boldsymbol{X}$ contains independent random variables which are normally distributed as $X_i \sim \mathcal{N}(\mu_i, \sigma_i)$, where μ_i, σ_i denote the mean value and standard deviation of X_i. These assumptions will be significantly relaxed later on.

One goal of uncertainty propagation is to compute the density of the outputs Y_t, Y_α, denoted as $\rho_{Y_t}, \rho_{Y_\alpha}$, based on the density of the inputs. In the case of normal distributions, it is sufficient to compute the mean value and variance of the output quantity, which, for a single noise source, is given as

$$\mu_{Y_\alpha} = \int_{\mathbb{R}^m} \mathcal{M}_\alpha(\boldsymbol{x})\, \rho_{\boldsymbol{X}_\alpha}(\boldsymbol{x})\, \mathrm{d}x, \tag{5}$$

$$\sigma^2_{Y_\alpha} = \int_{\mathbb{R}^m} (\mathcal{M}_\alpha(\boldsymbol{x}) - \mu_{Y_\alpha})^2\, \rho_{\boldsymbol{X}_\alpha}(\boldsymbol{x})\, \mathrm{d}x \tag{6}$$

For non-Gaussian distributions, the density can be reconstructed through the moment-generating function, if moments of all order are known. The moments given in (5) and (6) cannot be computed exactly in many cases as the model function $\mathcal{M}_\alpha$ is only given implicitly, through a parametric computer model. Hence, we are looking for numerical approximations, and three different approaches are considered in the following.

In a nutshell, one goal of uncertainty propagation is to compute the density of the outputs Y_t, Y_α, denoted as $\rho_{Y_t}, \rho_{Y_\alpha}$, based on the density of the inputs. To that aim, three different approaches are considered in the following: FOSM, Section III.B, evaluating the model at the nominal parameters; the MC approach, Section III.C, simply drawing and simulating a random sample; higher-order weighted quadrature, Section III.D, using quadrature points and weights to compute the mean value and standard deviations. Instead of a weighted quadrature, a PC surrogate approach may be used if entire distributions of the output are sought.

B. First-Order Second-Moment

The FOSM approximation, described for instance in [57], reads

$$\mu_{Y_\alpha} \approx \mu_{\mathrm{FOSM};Y_\alpha} = \mathcal{M}_\alpha(\boldsymbol{\mu}_{\boldsymbol{X}_\alpha}) + O(\sigma^2), \tag{7}$$

$$\sigma^2_{Y_\alpha} \approx \sigma^2_{\mathrm{FOSM};Y_\alpha} = \sum_{i=1}^{m_\alpha} \sigma_i^2 (\partial_{X_{\alpha,i}} \mathcal{M}_\alpha|_{\boldsymbol{\mu}_{\boldsymbol{X}_\alpha}})^2 + O(\sigma^3), \tag{8}$$

where $\boldsymbol{\mu}_{\boldsymbol{X}_\alpha} = (\mu_1, \mu_2, \ldots, \mu_{m_\alpha})$ and $\sigma = \max_i \sigma_i$. Also, O denotes a Landau symbol and $\partial_{X_{\alpha,i}} \mathcal{M}_\alpha|_{\boldsymbol{\mu}_{\boldsymbol{X}_\alpha}}$ refers to the partial derivative of $\mathcal{M}_\alpha$ with respect to $X_{\alpha,i}$, where the model is evaluated at the mean/nominal value $\boldsymbol{\mu}_{\boldsymbol{X}_\alpha}$. Hence, the model evaluated at the mean/nominal parameter value provides a second-order approximation of the mean value. Moreover, with the aid of the model sensitivities, a third-order approximation of the variance is obtained.

If $\mathcal{M}_\alpha$ is a linear function, Y_α is again normally distributed. This also remains approximately true if the model

is nonlinear but the input uncertainty small. In these cases, the FOSM method can be applied, since it is based on a first-order Taylor expansion. In [18], the FOSM approximation was applied to (3), which yields

$$\sigma_{Y_\alpha}^2 \approx \sigma_{\alpha;\text{inp}}^2 + \sigma_{\alpha;\text{mod}}^2 = \sum_{i=1}^{m_\alpha} \sigma_i^2 (\partial_{X_{\alpha,i}} \mathcal{M}_\alpha|_{\boldsymbol{\mu}_{\boldsymbol{X}_\alpha}})^2 + \sigma_{\alpha;\text{mod}}^2 \tag{9}$$

Then, FOSM can be applied again to propagate uncertainty to the total noise emission level Y_t (see equation (4)) as

$$\sigma_{Y_t}^2 \approx \frac{1}{(\sum_\alpha 10^{\mu_{Y_\alpha}/10})^2} \sum_\alpha 10^{\mu_{Y_\alpha}/5} \sigma_{Y_\alpha}^2 = \frac{1}{(\sum_\alpha 10^{\mu_{Y_\alpha}/10})^2} \sum_\alpha 10^{\mu_{Y_\alpha}/5} \left(\sigma_{\alpha;\text{inp}}^2 + \sigma_{\alpha;\text{mod}}^2 \right) \tag{10}$$

For a detailed description, the reader is referred to Refs. [18–20].

If the entire distribution of the output quantity is sought, i.e., ρ_{Y_t}, one can assume a normal distribution and employ the mean value and variance as outlined above. Hence,

$$Y_t \approx Y_{\text{FOSM},t} \sim \mathcal{N}(\mu_{\text{FOSM};Y_t}, \sigma_{\text{FOSM};Y_t}), \tag{11}$$

and the approximate density will be denoted as $\rho_{\text{FOSM};Y_t}$. FOSM is an intrusive method in the sense that the sensitivities/derivatives of the model function are required for each input parameter, but a non-intrusive implementation is also possible with finite difference approximations.

As outlined above, the main drawback of FOSM is the limitation to small input standard deviations. Moreover, the assumption of Gaussian distributions does not always hold in practice. Sampling and higher-order spectral methods may overcome these limitations. Sampling methods include MC, which is introduced below. However, their computational workload can be much higher than FOSM. Sampling methods easily require thousands of deterministic solutions, which cannot be afforded if the models are too complex. These limitations can be overcome PC surrogate methods, described further below.

C. Monte Carlo

The MC approach [4] simply draws a sample $\boldsymbol{X}_{\alpha,i} \sim \boldsymbol{X}_\alpha, i = 1, \ldots, I$, evaluates the model repeatedly as $Y_{\alpha,i} = \mathcal{M}_\alpha(\boldsymbol{X}_{\alpha,i})$ and then averages to approximate moments of the output random variable. The mean value and variance of Y_α can, for instance, be approximated as

$$\mu_{Y_\alpha} \approx \mu_{\text{MC};Y_\alpha} = \frac{1}{I} \sum_{i=1}^{I} Y_{\alpha,i}, \tag{12}$$

$$\sigma_{Y_\alpha}^2 \approx \sigma_{\text{MC};Y_\alpha}^2 = \frac{1}{I-1} \sum_{i=1}^{I} (Y_{\alpha,i} - \mu_{\text{MC};Y_\alpha})^2 \tag{13}$$

This approach is non-intrusive, i.e., it only requires the repeated simulation of the model with different input values. The accuracy of standard MC sampling is given as $O(I^{-1/2})$ (accuracy in the root-mean-square error) and hence, is independent of the number of random input variables. However, the convergence rate of $-1/2$ is inferior to other methods in many cases.

The uncertainty in the total emission can be handled in the same way, for instance, the mean value is approximated as

$$Y_t \approx \frac{1}{I}\sum_{i=1}^{I} 10 \cdot \log_{10}\left(\sum_{\alpha} 10^{Y_{\alpha,i}/10}\right) \tag{14}$$

Quasi-MC can improve the accuracy-efficiency ratio to some extent. In this work, we use point sets generated with Latin Hypercube sampling. We also combine the MC method with kernel density estimation to obtain a continuous approximation of the output density, written as

$$\rho_{Y_t}(y) \approx \rho_{\mathrm{MC};Y_t} = \frac{1}{I}\sum_{i=1}^{I} K_h(y - y_{t,i}), \tag{15}$$

where K_h denotes the Kernel (for instance, a normal kernel) with a suitably chosen smoothing parameter h and $y_{t,i}$ represents the realization of the random variable $Y_{t,i}$.

D. Weighted Quadrature and Polynomial Chaos

Like the previous section, we will distinguish between the computation of moments and the computation of the output density. In the former case, we will employ a weighted quadrature of higher-order (HO). In this case, we obtain the approximations

$$\mu_{Y_\alpha} \approx \mu_{\mathrm{HO};Y_\alpha} = \sum_{i=1}^{I} y_{\alpha,i} w_i, \tag{16}$$

$$\sigma^2_{Y_\alpha} \approx \sigma^2_{\mathrm{HO};Y_\alpha} = \sum_{i=1}^{I} (y_{\alpha,i} - \mu_{\mathrm{HO};Y_\alpha})^2 w_i, \tag{17}$$

where $y_{\alpha,i} = \mathcal{M}_\alpha(\boldsymbol{x}_{\alpha,i})$; $\boldsymbol{x}_{\alpha,i}$, and w_i represent the quadrature points and weights. It should be noted that the $\boldsymbol{x}_{\alpha,i}$ are selected in a deterministic way, whereas the $X_{\alpha,i}$ are random variables, which is reflected by lower case symbols. Common choices for $\boldsymbol{x}_{\alpha,i}$, and w_i are (weighted) Gauss or Clenshaw-Curtis quadrature [58]. More recently, the Leja quadrature is receiving increasing interest [59]. The most direct way to construct multivariate rules is to use tensor constructions. In this case, given a model function with a certain regularity k (k represents the decay rate of the Chebyshev polynomial expansion of $\mathcal{M}$ [60]), a weighted tensor rule converges as $O(I^{-k/n})$. Hence, the Monte Carlo method is preferred if $1/2 > k/n$, i.e., if there are many input parameters and the model function is not sufficiently regular.

If the entire distribution of the output quantity is sought, we employ a surrogate-based approach, the PCE, which can be roughly divided into intrusive and non-intrusive. The intrusive approach involves modifying the governing equations and software to estimate the PCE coefficients using a Galerkin projection [2]. In the context of software such as PANAM, which integrates several sub-modules, an intrusive approach would be cumbersome to realize, since modifications of various individual noise component models would be required. Instead, we pursue a non-intrusive approach, which enables to use existing software as a 'black-box' in a sampling approach. The non-intrusive PC approach can be further divided into several categories, namely: a) pseudo-spectral projection [61], b) stochastic point collocation [13], and c) PC decomposition with differentiation [62]. The pseudo-spectral projection technique involves finding the expectation of the product of the stochastic response and the multivariate basis orthogonal polynomials using quadrature methods or random sampling simulations. However, the number of function evaluations or samples required with quadrature methods increases exponentially with the increase in random input dimensions, commonly termed the '*curse of dimensionality*'. The curse of dimensionality can be alleviated by using sparse grids based on Smolyak's formula [63], but this also becomes unaffordable for high dimensional problems in terms of the computational cost. Currently, different adaptive least-squares approaches [64] and L1-minimization approaches [65] are being utilized to improve computational efficiency.

The PCE introduces a functional approximation of the form

$$Y_\alpha = \mathcal{M}_\alpha(\boldsymbol{X}_\alpha) \approx \mathcal{M}_{\alpha,n_\alpha}(\boldsymbol{X}_\alpha) = \sum_{i=0}^{n_\alpha} q_i \phi_i(\boldsymbol{X}_\alpha), \tag{18}$$

where q_i and ϕ_i refer to polynomial coefficients and basis functions, respectively. Alternatively, if a surrogate model for the overall emission is sought, we express Y_t as a PCE of all $\boldsymbol{X}_{\alpha;\mathrm{inp}}$ and $X_{\alpha,\mathrm{mod}}$. There are many common choices for ϕ_i, and the term PCE refers to the particular basis satisfying

$$\mathbb{E}[\phi_i \phi_j] = \delta_{ij}, \tag{19}$$

where we have assumed normalization, i.e., $\mathbb{E}[\phi_i^2] = 1$ for simplicity. Hence, the polynomials are adapted to the underlying probability distribution. One of the main advantages of the PC basis, compared to other polynomial bases, is the statistical information that can be obtained directly from the coefficients. In particular, the polynomial coefficients allow to compute moments and Sobol's sensitivity indices directly; see [66] for details. To approximate the output distribution, we sample the PC expansion and employ kernel density estimation again; the resulting approximation is denoted as $\rho_{\mathrm{PC};Y_\alpha}$. Evaluation of polynomials can be carried out at negligible cost; hence, the only relevant computational effort results from the construction of the PC approximation, for which we employ orthogonal matching pursuit [65], which is a sparse adaptive least square approximation.

E. Imprecise Stochastic Setting

In practice, the given data are often insufficient to justify working with a perfectly-known distribution of the input parameters. Hence, in this case, the approaches outlined in the preceding sections require some modifications. Also, in the PANAM model, where sub-models from different sub-disciplines are aggregated, it is unlikely that a sufficient amount of data are available to precisely infer all relevant distributions. This concerns the entire joint distribution of input parameters, both their individual marginal distributions and the model input parameter dependence. Commonly, independence is assumed in such a case, which, however, if not met, may significantly alter the results and underestimate tail probabilities, see for instance [67].

Here, we employ random variables for all uncertainties, both epistemic and aleatoric. An interval approach is applied to handle uncertainty in the hyper-parameters of the input distributions. An overview of existing alternatives can be found, for instance, in [68]. In particular, we propose to use probability-boxes (p-boxes) to handle both imprecision in the marginals and the dependence structure. P-boxes belong to imprecise probabilistic models and are closely connected to Dempster-Shafer (or evidence) theory [67]. The notation here closely follows [69] (see there for a detailed background on p-boxes).

We denote with $\boldsymbol{X}$ (without subscripts) the collection of all uncertain input variables. P-boxes are commonly introduced via the cumulative distribution function (CDF) instead of the probability density function (PDF). The CDF is defined as

$$F_{\boldsymbol{X}}(\boldsymbol{c}) = P(\boldsymbol{X} \leq \mathbf{c}) \tag{20}$$

which is connected with the PDF as $\rho_{\boldsymbol{X}} = \frac{\partial^m F_{\boldsymbol{X}}}{\partial c_1 \cdots \partial c_m}$. The distribution parameters $\boldsymbol{\theta}$, (for instance $\boldsymbol{\theta} = (\mu, \sigma)$ in case of a normal distribution) are typically assumed to be known. If the data are insufficient to infer these parameters precisely, they can be modeled to belong to a set as $\boldsymbol{\theta} \in D_\theta \subset \mathbb{R}^n$. Since for each $\boldsymbol{\theta}$ we obtain a different CDF, a p-box consists of a family of distributions, constrained by the upper and lower envelope

$$\underline{F}_{\boldsymbol{X}}(\boldsymbol{x}) = \min_{\boldsymbol{\theta} \in D_{\boldsymbol{\theta}}} F_{\boldsymbol{X}}(\boldsymbol{x}|\boldsymbol{\theta}), \qquad \overline{F}_{\boldsymbol{X}}(\boldsymbol{x}) = \max_{\boldsymbol{\theta} \in D_{\boldsymbol{\theta}}} F_{\boldsymbol{X}}(\boldsymbol{x}|\boldsymbol{\theta}), \tag{21}$$

where $F_{\boldsymbol{X}}(\boldsymbol{x}|\boldsymbol{\theta})$ denotes the CDF, conditional on a specific value of $\boldsymbol{\theta}$. Our model for the joint CDF reads as

$$F_{\boldsymbol{X}}(\boldsymbol{x}|\boldsymbol{\theta}) = F_{\mathrm{C}}(F_{X_1}(x_1|\boldsymbol{\theta}_1), F_{X_2}(x_2|\boldsymbol{\theta}_2), \ldots, F_{X_n}(x_n|\boldsymbol{\theta}_n)|\boldsymbol{\theta}_{\mathrm{C}}), \tag{22}$$

where F_{C} signifies a copula dependence model, see, for instance [70–73]. Hence, $\boldsymbol{\theta}_i$, and $\boldsymbol{\theta}_{\mathrm{C}}$ represent the interval (hyper)-parameters for the marginal distributions and the dependence, respectively. The copula approach allows to introduce p-boxes for dependence modeling, which is much less explored than p-boxes for marginal distributions.

Since the focus is on uncertainty assessment for aircraft noise prediction, we only summarize the remaining steps

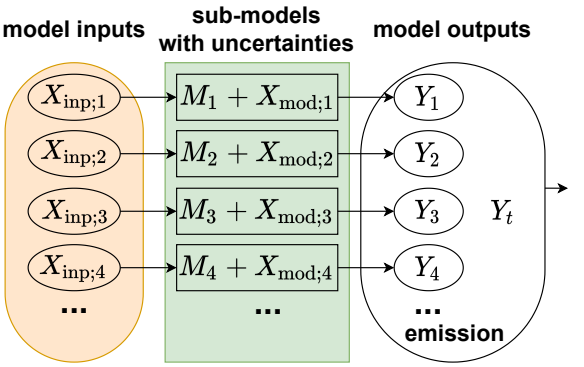

Fig. 2 Visualization of the noise emission modeling with uncertain parameters in the flight point loop.

of p-box modeling and refer to Appendix A for a more detailed description. For the dependence model, a Gaussian copula is used, which is parametrized by a correlation-like matrix $\boldsymbol{R}$ with entries $r_{ij} \in [-1, 1]$. In particular, choosing $r_{ij} = 0$ for $i \neq j$ results in the independent case. This represents distributional p-boxes, which are parametric with interval-valued parameters.

In analogy to the standard probabilistic setting, where the input distribution needs to be propagated to the model output, the input p-boxes also need to be propagated. Various algorithms such as an interval MC method [74] and PC techniques [69] can be used to this end. However, these algorithms typically assume independence of the model inputs and it is unclear how to combine them with imprecise copulas. Here, we use a dedicated Latin Hypercube sampling algorithm to approximate the output p-box $\underline{F}_{Y_t}$ and $\overline{F}_{Y_t}$ (see Appendix A). For computational efficiency, a PC surrogate model is used here instead of the original PANAM noise model. This step introduces an additional approximation, which needs to be controlled carefully together with the sampling error.

F. Implementation

In Figure 2, an uncertainty propagation overview is sketched. The model input parameters are depicted in orange, the green block contains the noise sub-models implemented in PANAM, together with the model uncertainties. The last block in white represents energetic summation of the individual source noise levels. Uncertainty quantification with the PANAM tool can be carried out in an intrusive and a non-intrusive way. An intrusive FOSM approach has been developed previously and is described in more detail in Ref. [18]. This work complements these efforts with non-intrusive methods for UQ, that require multiple simulation runs. To that end, the PANAM code has been updated to process input ($X_{\text{inp},i}$) and model parameter ($X_{\text{mod},i}$) variations for every noise source model. For each of the perturbed values a PANAM simulation run produces the associated output quantities Y_i and Y_t. This data are collected in the so-called experimental design, which is used to carry out Monte Carlo simulation and adaptive surrogate modeling. The surrogate model can then be used to perform all aforementioned UQ tasks, such as estimating moments and distributions and propagating p-boxes, without further recurrences to the PANAM code. It should be noted that the choice of relevant

input and model parameters is based on simulation experience in this work. A more comprehensive and automated selection could be based on (global) sensitivity analysis in the future, which may results in a different set of relevant parameters. The next section gives some first indications in this direction.

IV. Results: Test Case Applications

This section provides the details of the air operation scenarios and relevant parameters and dependencies considered in the study. Then, numerical results are reported. Please recall that we consider the approach and departure situation only at one single and fixed emission angle of 60° (see Figs. 1(a) and 1(b)) in a reference distance of 1 m. The sound pressure levels of the test cases are given in Section II. Note that all results presented in this section are conditional on the emission angle. Totally different results may be obtained if another metric, emission angle or scenario is considered. The authors main intention is to illustrate which results can be obtained with the UQ methods, particularly the PC method, presented in Section III.

In the context of this research, we consider two different settings. First, we consider uncertainties in the parameters $X_{\text{mod};\alpha}$ and their propagation to the total emission level via Eq. (4), which is called the **model uncertainty** case. The considered source models with associated modeling uncertainties are summarized in Table 1. The uncertainties reflect possible simplifications of modeling the noise source emissions and the main interest of the model uncertainty case is to illustrate the different approaches using a simple setting (presented in Section IV.A). The second test case, referred to

Table 2 Selected uncertain model inputs $\boldsymbol{X}_{\alpha;\text{inp}}$ for each source model Y_α as defined in [18]

Source model Y_α	Input parameter $\boldsymbol{X}_{\alpha;\text{inp}}$	Standard deviation $\sigma_{\alpha;\text{inp}}$	Absolute values (approach / departure), unit
Airframe sources	TAS ($X_{\text{af};1}$)	±8 %	74.8 ± 6.0 / 86.0 ± 6.9, m/s
	t.e. sweep angle ($X_{\text{af};2}$)	±0.5 °	segment sweep angle ±0.5, °
	l.e. sweep angle ($X_{\text{af};3}$)	±0.5 °	segment sweep angle ±0.5, °
	wing loading ($X_{\text{af};4}$)	±10 %	477.9 ± 4.8 / 496.1 ± 5.0, kg/m^2
Fan	N1 ($X_{\text{fan};1}$)	±10 %	41.5 ± 4.2 / 73.8 ± 7.4, rpm
	RSS ($X_{\text{fan};2}$)	±5 %	2.0 ± 0.1, %
	total mass flow ($X_{\text{fan};3}$)	±10 %	202.0 ± 20.2 / 355.7 ± 35.6, m/s
	relative tip Mach ($X_{\text{fan};4}$)	±1 %	0.713 ± 0.007 / 1.301 ± 0.013, -
Jet	core exhaust velocity ($X_{\text{jet};1}$)	±8 %	123.8 ± 9.9 / 312.4 ± 25.0, m/s
	bypass exhaust velocity ($X_{\text{jet};2}$)	±5 %	148.7 ± 7.4 / 259.4 ± 13.0, m/s
	TAS ($X_{\text{jet};3}$)	±8 %	74.8 ± 6.0 / 86.0 ± 6.9, m/s
	total jet core exhaust temp. ($X_{\text{jet};4}$)	±10 %	605.8 ± 6.1 / 664.0 ± 6.6, K

as **combined model and input uncertainties**, considers both modelling uncertainty of the total emission, $L_{\text{em},t}$, and input uncertainty and hence the entire PANAM modeling chain. Input uncertainties caused by incomplete knowledge of the precise parameter values or natural variability further contributes to the uncertainty of the predicted noise

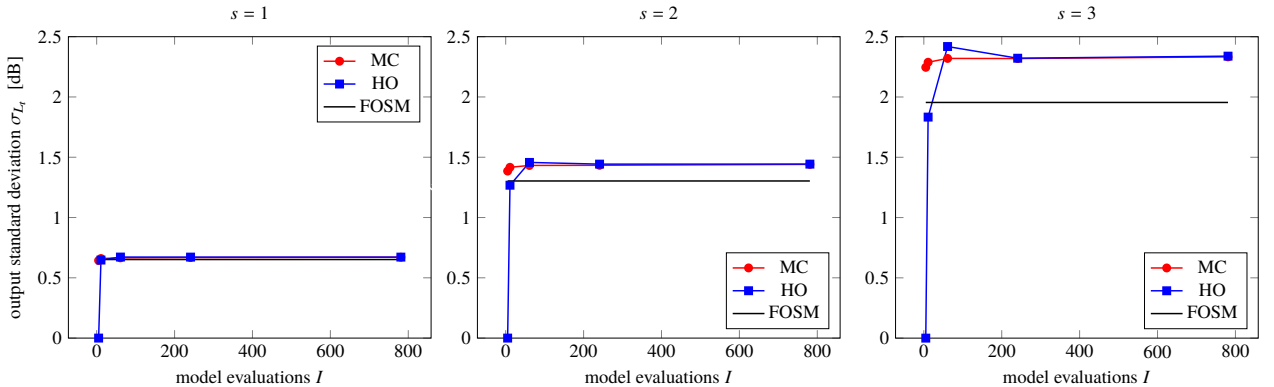

Fig. 3 Comparison of computed standard deviations with FOSM, higher-order (HO) quadrature, and Monte Carlo method (MC) for $s = 1, 2, 3$ and the approach scenario.

emission. Relevant input parameters and their uncertainty are listed in Table 2. The selected parameters capture the most dominating effects on the predicted noise levels, according to prior simulation experience.

It should be noted that some input parameters given in Table 2 are correlated (linear or higher-order), e.g., the engine mass flow and fan tip Mach number are related to the flight velocity. This dependence is neglected when performing a FOSM evaluation. However, we will account for this dependence when assessing higher-order uncertainty methods with an imprecise copula model, which allows computing bounds on the effect of all possible dependencies on the overall system noise uncertainty, shown in Section IV.B.

A. Model Uncertainty

First step: mean values and standard deviations. We consider the approach scenario. The input uncertainties are neglected to account for modeling uncertainty only. All random variables are assumed to be normally distributed as $X_{\text{mod};\alpha} \sim \mathcal{N}(\mu_\alpha, \sigma_\alpha)$, where $\sigma_\alpha = s\sigma_{\alpha,0}$ and $\sigma_{\alpha,0}$ correspond to the uncertainties given in Table 1. Note that we introduce a parameter s to equally scale all the considered uncertainties. This allows to analyze the accuracy of the different methods for different sizes of uncertainties. The mean values are chosen to be identical to the nominal values, reported earlier. We compare FOSM to the HO quadrature and MC sampling method for different sizes of the input uncertainty. This allows establishing a range of applicability for the FOSM approach. Figure 3 depicts the computed standard deviations for the total emission $L_{\text{em,t}}$. We observe that the HO and Monte Carlo values agree well after a few hundred model evaluations I. The difference between these two methods and the FOSM approach increases with larger values of s. Even for a large deviation corresponding to $s = 3$, the FOSM result is off by less than 1 dB, which is acceptable in many applications.

Figure 4 shows the associated errors for $s = 1, 2, 3$. The MC errors have been computed 200 times to remove randomness from the results, and only the average error is shown here. For a fixed number of sampling points, the accuracy of the MC and HO methods decreases as s increases, which is expected as a broader parametric domain needs

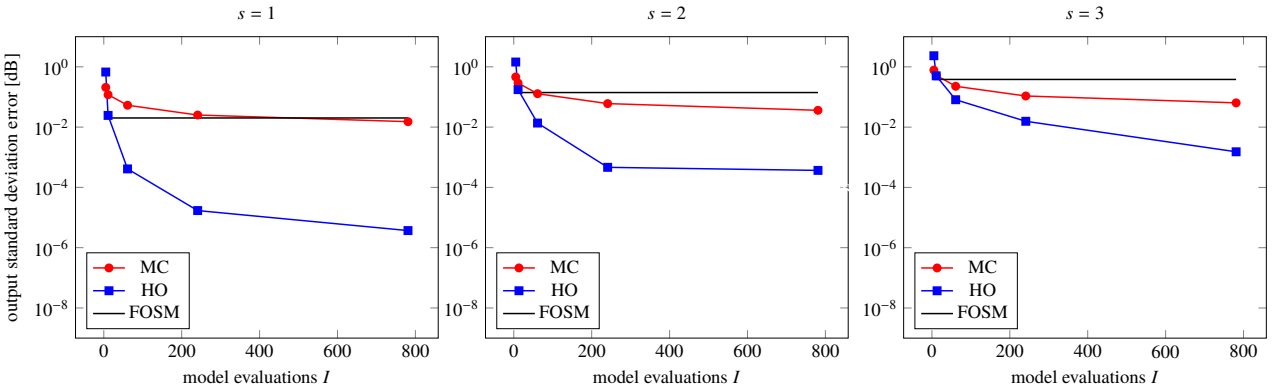

Fig. 4 Comparison of computed standard deviation errors with FOSM, higher-order (HO) quadrature, and Monte Carlo (MC) method for $s = 1, 2, 3$ and the approach scenario. The errors are computed with respect to a quadrature rule with an accuracy of ten digits.

to be captured. Also, the FOSM accuracy deteriorates with increasing s, which is again expected, as it is based on a first-order Taylor expansion, which is limited to small input uncertainties. These results further reveal the improved accuracy provided by the HO quadrature approach compared to MC sampling. This advantage, well-known in the uncertainty literature [75], will deteriorate if the number of uncertain parameters grows. All these numerical experiments have been repeated for the departure setting; however, as the results and implications are qualitatively similar, the figures have been moved to Appendix B.

To reveal the dependence of the different methods on the size of uncertainties, in Fig. 5 the computed standard deviations (left) and errors (right) for FOSM and the HO quadrature approach are depicted. The MC results are not reported since they are qualitatively similar to the HO results with $I = 61$, which corresponds to a quadrature grid of total degree two. We additionally provide results for a degree one grid, which is expected to be close to the first-order Taylor expansion-based FOSM computation. The accuracy of the FOSM and degree one quadrature results are indeed comparable. The degree two grid provides better accuracy, in particular for larger uncertainties. Finally, it should be noted that both FOSM and degree one quadrature underestimate the output uncertainty. We are not aware of any systematic justification of this result.

Second step: ouput distributions. Distributions can be compared with violin plots, for instance, which show the PDF on the $y-$axis. In Figure 6 we depict the output distributions obtained with the three different methods. Clearly the uncertainty increases with the scaling factor s from left to right. Additionally, the distribution deviates more and more from a normal distribution. In particular, the densities slightly shift towards higher noise levels and become skewed, for $s = 3$. Both MC and HO approaches are able to capture such a non-Gaussian PDF, whereas the FOSM PDF remains normally distributed, by assumption. A quantitative difference between the different PDFs can be computed with the Kullback-Leibler divergence, which evaluates the difference between the FOSM output density and the MC reference as $D_{\mathrm{KL}}(\rho_{\mathrm{FOSM};Y}||\rho_{\mathrm{MC};Y}) = 0.0471, 0.1982, 0.7781$ for $s = 1, 2, 3$, respectively. One can also see the deviations in the

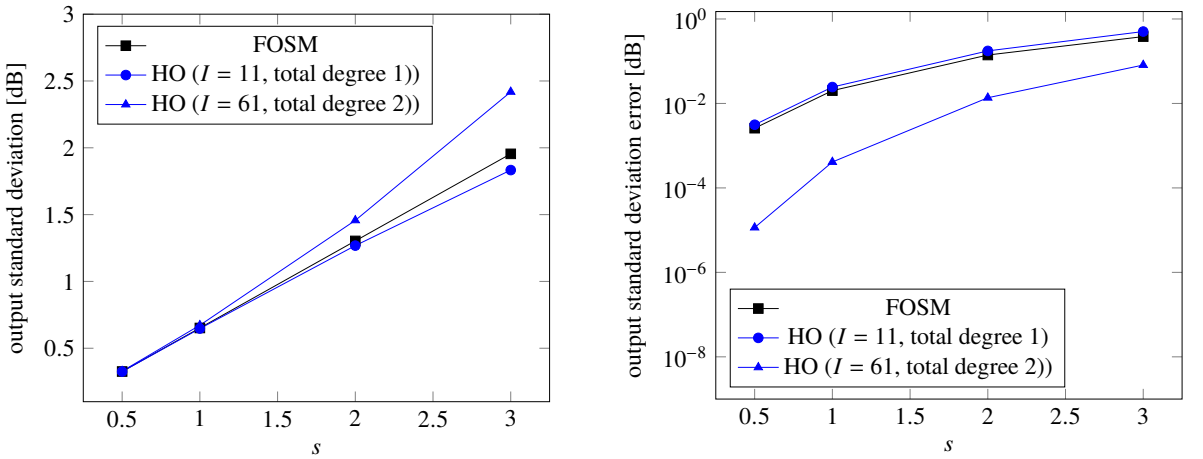

Fig. 5 Output uncertainties standard deviations (left) and errors in standard deviations (right) for FOSM and higher-order (HO) weighted quadrature with variable number of model evaluations for uncertainty magnitudes scaled by s for the approach scenario.

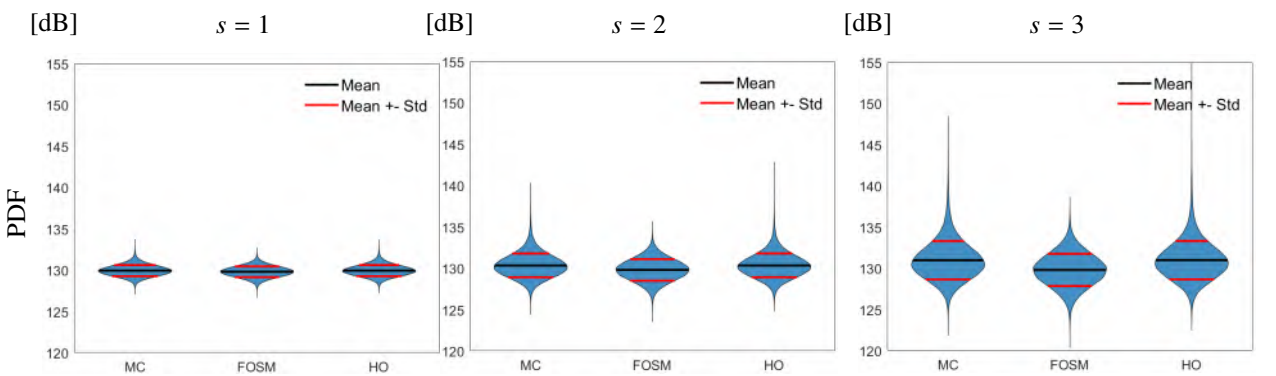

Fig. 6 Violin plots for the approach scenario. Mean values are depicted with solid black lines; the red lines represent the mean values plus/minus one standard deviation.

computed standard deviations (red line) between the different methods, particularly for high values of s.

The different PDFs have been computed as follows. For the FOSM approach, normal distributions with the computed mean values and standard deviations have been assumed. For both MC and HO approaches, kernel density estimation is employed with a Gaussian kernel based on a sample of the output quantity. Here, 10^5 realizations of the total emission have been used to obtain the kernel density estimates.

Third step: p-box approach. We now apply p-boxes, as outlined in Section III to take into account a limited knowledge about distributions and correlation. Quite often the only available information about the probability distribution are estimates of the mean value and standard deviation. Therefore, we propose to construct a distributional p-Box, which contains CDFs of variable shape, with the same mean value and standard deviation. The Beta distribution offers this type of flexibility. Hence, we assume that every random variable is Beta-distributed $X_i \sim \mathcal{B}(a_i, b_i, \alpha_i, \beta_i)$, where $[a_i, b_i]$ represents the support of the distribution and α_i, β_i the shape parameters. For more details, please refer

to Appendix A. We assume symmetry of the distribution by setting $\alpha_i = \beta_i \in [1.5, 5]$, but a possible skew-symmetry of the distribution could also be considered through $\alpha_i \neq \beta_i$. The parameter correlation matrix $\boldsymbol{R}$ of the Gaussian copula model is set to the identity matrix with a single off-diagonal term $r_{4,5} = r_{5,4} \in [-1, 1]$. Hence, we assume all model uncertainties from different noise sources to be independent, except for the trailing and leading edge models (Table 1), for which the strength of the dependence is controlled with $r_{4,5}$. In Figure 7 we show the inferred p-boxes of the total emission. On the left, imprecision in the dependence is accounted, whereas on the right, both the imprecision in the parameter distribution and the dependence are taken into account. Several Monte Carlo simulations are plotted here, where the interval parameters are as follows: $r_{4,5}^{(k)} \sim \mathcal{U}(-1, 1)$ and $\alpha_i \in \mathcal{U}(1.5, 5)$, where $\mathcal{U}$ refers to a uniform distribution; samples are drawn from these intervals and a standard uncertainty propagation problem is solved to obtain a CDF. Hence, this result reflects the uncertainty in the uncertain system's response, which should be bounded by the output p-box, as long as the Latin Hypercube sample size has been chosen large enough. This is indeed the case for the samples shown in Fig. 7. The optimization problems are solved by computing the minimum and maximum over a large number of samples in the domain spanned by the interval parameters. We employ the PC surrogate model to propagate the p-box as outlined in Appendix A. Note that in this way, a large number of samples can be afforded since in addition to surrogate modeling only (small-scale) Cholesky factorizations and inversions of CDFs are needed. The evaluations of the polynomial surrogate model can be neglected from an efficiency point of view. The Latin Hypercube sample size has been set to 10000 in both cases of Fig. 7.

In Fig. 7, it can also be observed that accounting for additional imprecision in the dependence increases the envelope of the output p-box, as expected. From an application perspective, it could be interesting to extract information about exceedance probability from such results. For instance, the probability of obtaining a noise level below 130 dB would lie in an interval spanned by the intersection of the p-box envelope and the vertical line at 130 dB. A design considering all sources of imprecision results in larger intervals and requires more robust noise reduction measures to achieve the design goal (noise level < 130 dB) with certainty.

B. Combined Model and Input Uncertainties

If not only model uncertainty (Section IV.A), but also input uncertainties should be taken into account, a large set of random variables needs to be considered, which is summarized in a vector as

$$\boldsymbol{X} = [X_{\text{mod;jet}}, X_{\text{mod;fan}}, X_{\text{mod;gear}}, X_{\text{mod;t.e.}}, X_{\text{mod;l.e.}}, X_{\text{af;1}}, X_{\text{af;2}}, X_{\text{af;3}}, X_{\text{af;4}}, X_{\text{fan;1}}, X_{\text{fan;2}}, X_{\text{fan;3}}, X_{\text{fan;4}}, X_{\text{jet;1}}, X_{\text{jet;2}}, X_{\text{jet;4}}]. \tag{23}$$

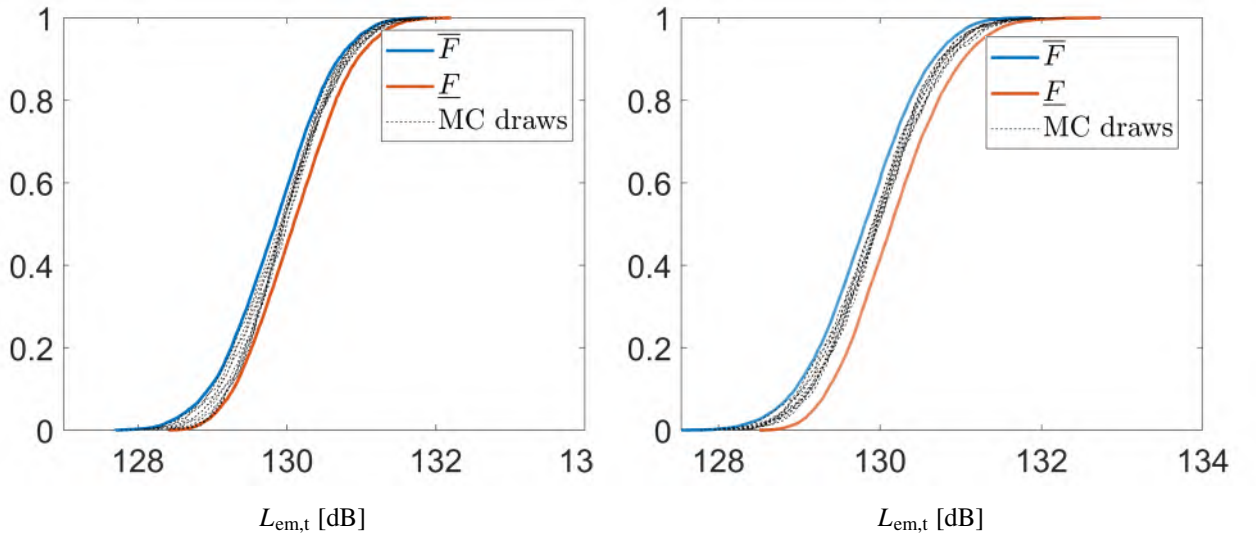

Fig. 7 Imprecise probabilities for the approach scenario and $s = 1$. (Left) probability density function (PDF) for different shape parameters of Beta distribution and $X_{\mathrm{mod,jet}}$. (Right) propagated output p-box for $L_{\mathrm{em,t}}$ taking into account both imprecise PDF and copula.

Table 3 Moments computed with the FOSM, MC, and PC method for the approach scenario. For PC 1900 simulation runs were used to estimate a sparse basis with 195 polynomials. The errors reflect the cross-validation error and root-mean-square error for the PC and MC methods, respectively.

Method	Solver calls I	Mean value [dB]	Standard deviation [dB]	Error [dB]
FOSM	–	129.908	1.129	-
MC	2000	130.176	1.437	0.032
PC	1900	130.200	1.420	$< 10^{-3}$

Since the TAS parameter appears twice, the entry $X_{\mathrm{jet};3}$ is omitted. Note that $\boldsymbol{X}$ contains both model parameters and parameters which represent model uncertainty. All parameters are represented as

$$X_i = \mu_i(1 + \tilde{X}_i),\ i = 1, \ldots, 16, \tag{24}$$

where $\mathbb{E}[\tilde{X}_i] = 0$ such that

$$\mathbb{E}[X_i] = \mu_i, \quad \sigma[X_i] = \mu_i \sigma[\tilde{X}_i] \tag{25}$$

Thus, all uncertainties are characterized through μ_i and $\sigma[\tilde{X}_i]$, where the latter refers to the parameter standard deviation, relative to the mean value. All values can be found in Table 2. For the model uncertainties $X_{\mathrm{mod};\alpha}$, $s = 1$ has been set throughout this subsection, and the same emission angles as in Section IV.A are used.

In the first simulation, reported in Table 3 and Table 4, the moments computed with all three methods are compared. For the sampling-based methods (PC and MC), we generate Latin Hypercube samples, assuming independence, and

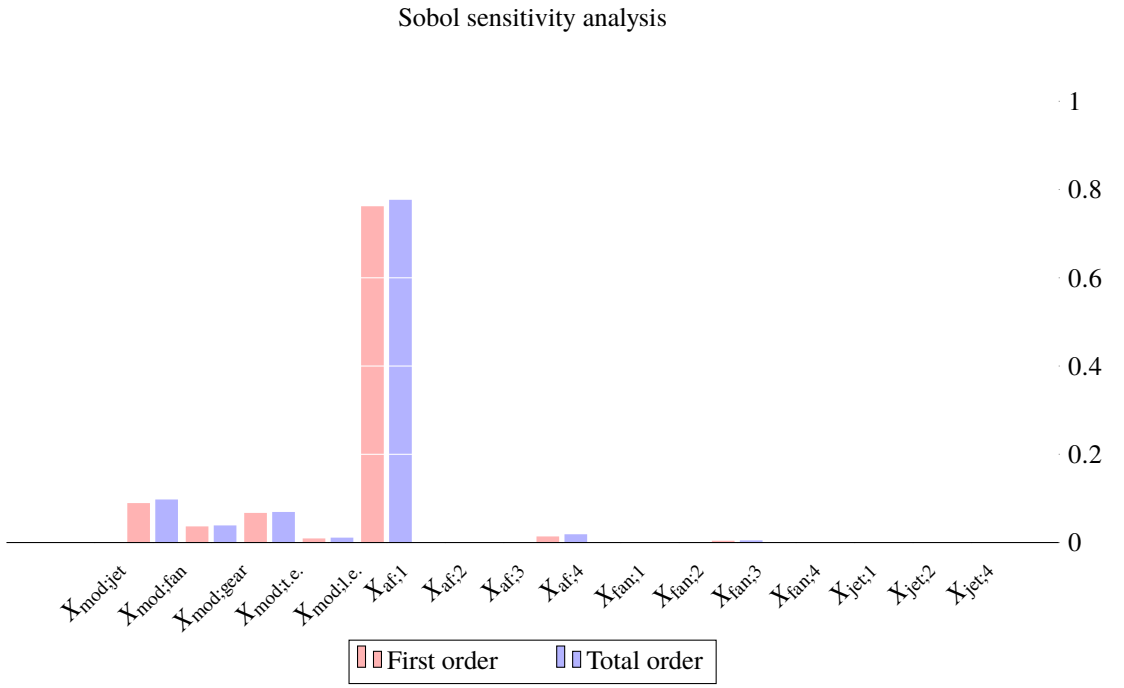

Fig. 8 Sobol sensitivity analysis for the approach scenario. First-order sensitivity indices and total order indices are displayed.

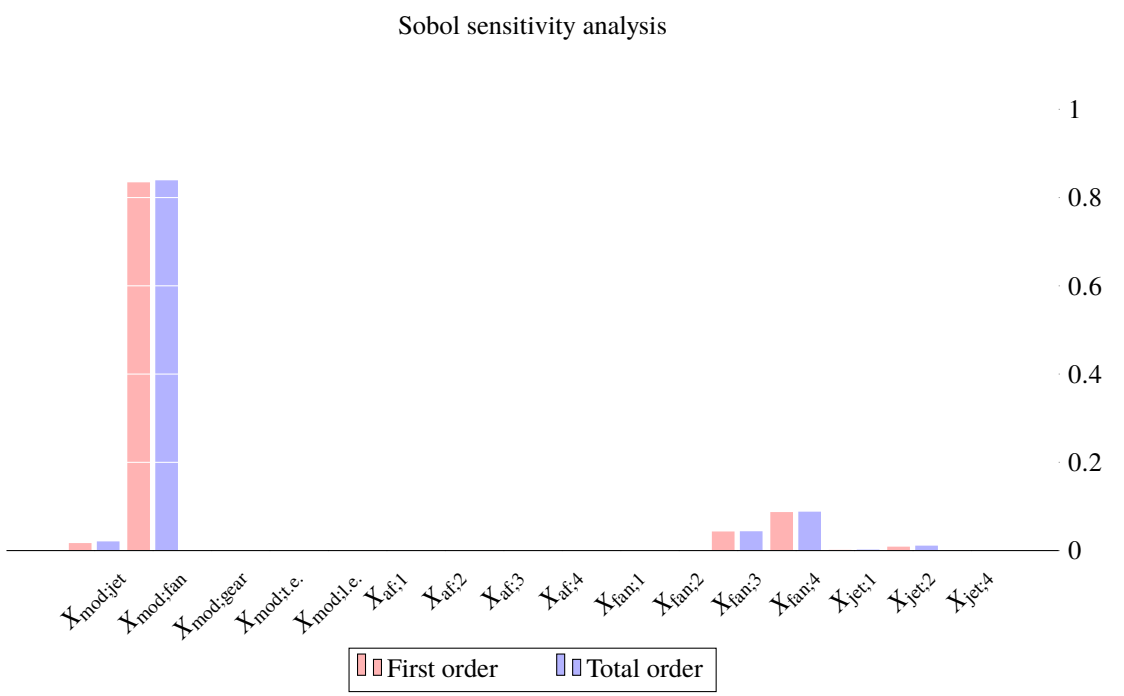

Fig. 9 Sobol sensitivity analysis for the departure scenario. First-order sensitivity indices and total order indices are displayed.

Table 4 Moments computed with the FOSM, MC, and PC method for the departure scenario. For PC 1900 **simulation runs were used to estimate a sparse basis with** 104 **polynomials. The errors reflect the cross-validation error and root-mean-square error for the PC and MC methods, respectively.**

Method	Solver calls I	Mean value [dB]	Standard deviation [dB]	error [dB]
FOSM	–	139.496	1.769	–
MC	2000	139.696	1.840	0.0412
PC	1900	139.766	1.802	$< 10^{-3}$

call the PANAM code for the realizations $\{\boldsymbol{X}^{(i)}\}_{i=1}^{I}$. As a result, realizations of the output $\{Y_t^{(i)}\}_{i=1}^{I}$, i.e., the total emission are obtained. The input-output pair is called the experimental design and is used to estimate the PC coefficients and the Monte Carlo moments. The sample size $I \approx 2P$ is chosen, where P denotes the total number of multivariate polynomials used. For PC analysis, the OMP implementation of UQLab [76] is employed to obtain an adaptive, sparse, and regression-based estimation of the PC coefficients. The surrogate model with P polynomials is denoted as $\mathcal{M}_P$. The accuracy of the so-obtained PC expansion is assessed through cross-validation, where a new experimental design $\{\boldsymbol{X}^{(i)}, Y^{(i)}\}_{i=1}^{I_{\mathrm{CV}}}$, is used at which the relative, empirical, mean-square error is computed

$$\text{rel. CV error } = \frac{\sum_{i=1}^{I_{\mathrm{CV}}} (\mathcal{M}(\boldsymbol{X}^{(i)}) - \mathcal{M}_P(\boldsymbol{X}^{(i)}))^2}{\sum_{i=1}^{I_{\mathrm{CV}}} (\mathcal{M}(\boldsymbol{X}^{(i)}) - \mu_Y)^2} \tag{26}$$

It is observed that all three methods agree well with regard to the predicted moments. For the PC surrogate, a degree $P = 3$ is used, which yields a small error. The Monte Carlo error is slightly larger, even if almost the same number of simulations are employed. This can be attributed to the fact that the PC surrogate model leverages anisotropy in the model. Although the FOSM errors are the highest in both cases, compared to the PC reference, the method predicts the proper orders of magnitudes. Note that since FOSM is not sampling-based, a number of solver calls and errors are not reported.

PC surrogate models further permit to extract Sobol sensitivity indices [66], which allows generating data acquisition plans to reduce the overall uncertainty. The results are reported in Fig. 8 and Fig. 9. For the approach scenario and the considered emission angle, the TAS uncertainty contributes most to the output uncertainty, followed by the modeling uncertainties in the noise models. In the departure scenario, however, the modeling uncertainty in the fan model dominates the emission uncertainty. It should also be noted that, in both cases, the first order indices are almost identical to the total order indices, which indicates that only mild nonlinearities are present in the model for the given input uncertainty magnitude.

Final step: Scenario comparison. To compare different scenarios of uncertainties with different settings, in Figure 10 we depict violin plots for the uncertainty in the total emission for the approach scenario (left) and the departure scenario (right). On the left, we compare the combined input/model uncertainty case against the model uncertainty

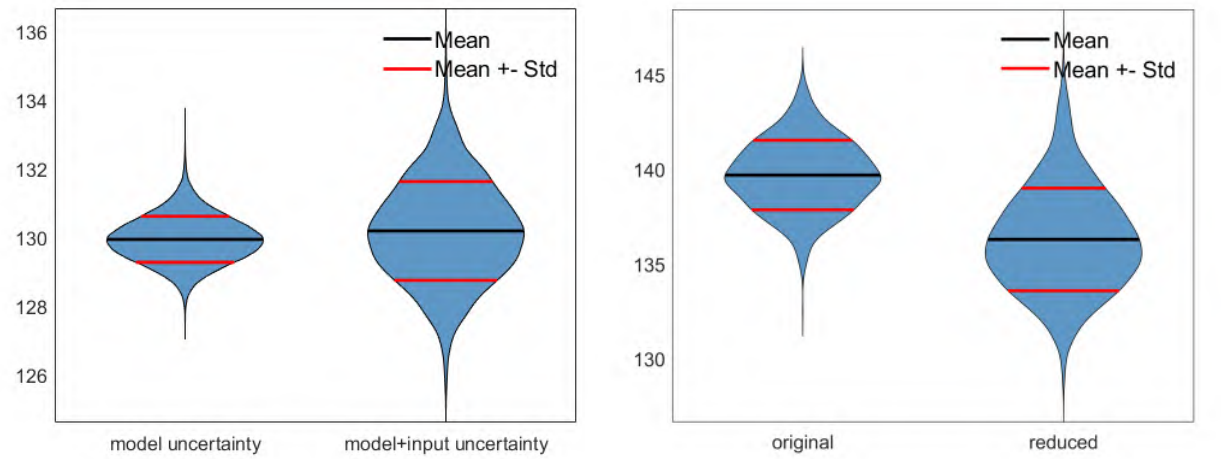

Fig. 10 Comparison of uncertainties for different settings/scenarios, represented through violin plots. (Left) uncertainties in the approach scenario for combined model and input uncertainties and the case of model uncertainties only. (Right) uncertainties in the departure scenario for input uncertainties as given in Table 2 compared to a new technology scenario with reduced fan mean value but larger uncertainties.

case for $s = 1$. One can observe that the additional uncertainties in the combined uncertainty case amplify the output standard deviation. On the right side, a technology comparison is mimicked, where the uncertainties as defined in Table 2 are referred to as *original*. They are compared to a setting (*reduced*) where the fan has a reduced mean value (-5 dB), but with two times larger standard deviation than the original. This may represent a future fan technology with improved sound design, which can be less accurately captured with our existing models and hence requires a larger model uncertainty. The modified fan setting reduces the mean value but increases the uncertainty of the total emission vastly. Also, the shape of the violins shows a non-Gaussian profile, which requires the application of a sampling-based approach or higher-order methods.

V. Discussion

The reported numerical results substantiate previous attempts to quantify uncertainty in aircraft noise with the FOSM method [18]. When the analyst is interested in obtaining rough estimates of the output moments, the FOSM-errors are in an acceptable range. At the same time, the additional computational effort only consists in estimating the model sensitivities, which is promising, in particular for complex simulation cases. On the other hand, if additional information, e.g., the output distribution or exceedance probabilities are sought, higher order surrogate modeling is beneficial. With the PC expansion in particular, arbitrary small approximation errors can be obtained at a moderate additional computational effort. Although MC sampling achieves comparable accuracies, more sampling points are needed. The PC method should also be chosen if the input uncertainty is very large in order to accurately capture non-Gaussian output distributions. We also observe that missing statistical input information can have a relevant impact on the results.

Hence, detailed information on the input uncertainties is required, in particular for computing tail probabilities.

A future study should consider the more challenging scenario of predicting the entire system noise, i.e., from the emission of the noise, via the propagation through the turbulent atmosphere, down to the noise levels as received on the ground. Indeed, the present results have been obtained for a single emission only, neglecting propagation uncertainties and complete flight scenarios. Since, in the general case, the associated parameter space will be much larger, the applicability of higher order surrogate modeling is yet to be established. As a promising direction, the global sensitivity analysis reported in this study suggests a strong anisotropy of the parameter space, which could be further exploited. Yet, another challenge in the general case are the parameter correlations between the emission spectral at neighboring flight points, which need to be taken into account.

VI. Conclusion and Outlook

This paper reports a comprehensive study on uncertainty propagation for aircraft noise emissions. Different methods, already in use in the community, are compared and jointly applied for the first time to a real aircraft system noise prediction test case. The FOSM method persists as a cheap alternative with acceptable accuracy to estimate low-order moments. The Polynomial Chaos expansion on the other hand allows to obtain accurate surrogate models, which can be used for various tasks, including uncertainty quantification with limited statistical input data. Uncertainty quantification is of major importance for decision making, when new technologies need to be assessed virtually. Assessing uncertainties will also gain in relevance for model selection and fusing heterogeneous simulation and measurement data of sub-models with variable fidelity.

Future studies should consider uncertainty quantification for the entire aircraft system noise assessment. Handling large parameter spaces and correlation will be a key challenge in this case, which could be addressed by systematically identifying large input sensitivities for variable selection and reduction of input uncertainties through additional measurements and simulations. One aim is to routinely carry out uncertainty quantification for aircraft noise simulation whenever simulation results are compared to experimental data. Only then, a meaningful and comprehensive comparison is enabled. Future application cases will also focus on mixed fidelity simulation processes, where different tools and experimental data input are processed simultaneously. Furthermore, based on the knowledge of underlying uncertainties, it will become possible to choose the required model and input data quality for a certain simulation task.

Acknowledgments

Part of the DLR work package was financed by the Deutsche Forschungsgemeinschaft (DFG, German Research Foundation) under Germany's Excellence Strategy—EXC 2163/1—Sustainable and Energy Efficient Aviation—Project-ID 390881007. The cooperation among the institutions was initiated with the "Workshop on UQ4Acoustic Simulations", December 3-4, 2018, TU Braunschweig, Germany and partly funded by the SFB 880 at TU Braunschweig. The work

received no additional external funding; the internal funding by the authors' institutions TU Braunschweig, DLR, UA and Empa is gratefully acknowledged.

Appendix A: Details of the Imprecise Stochastic Setting

Any continuous multivariate CDF can be written as

$$F_{\boldsymbol{X}}(\boldsymbol{x}) = F_{\mathrm{C}}(F_{X_1}(x_1), F_{X_2}(x_2), \ldots, F_{X_n}(x_n)), \tag{27}$$

see [77], where the copula F_{C} contains all information regarding parameter dependence. Since $F_{X_i}(X_i) \sim \mathcal{U}(0,1)$, i.e., $F_{X_i}(X_i)$ is uniformly distributed in $[0,1]$, a copula is nothing else than a CDF on $[0,1]^n$. Choosing a copula is hence, equivalent to choosing a dependence model. This model selection procedure can be based on cross-validation, if sufficient data are available. If such data are lacking, so-called Fréchet Hoeffding inequalities can be used [67] to obtain bounds on all possible dependence models. Here, a parametric approach is employed, which consists of choosing a copula family with interval-valued parameters. This approximation does not guarantee to obtain strict upper bounds on the dependence imprecision. The approach is merely for convenience, to allow for efficient sampling strategies, in particular. We introduce two parameter vectors $\boldsymbol{\theta} = (\boldsymbol{\theta}_1^\top, \boldsymbol{\theta}_2^\top, \ldots, \boldsymbol{\theta}_n^\top)^\top \in D_n$ and $\boldsymbol{\theta}_{\mathrm{C}} \in D_{\mathrm{C}}$, where $\boldsymbol{\theta}_i$ and $\boldsymbol{\theta}_{\mathrm{C}}$ contain the unknown parameters of $F_{X_i}(X_i)$, and correlation (dependence) parameters, respectively. With this notation at hand, the parametric CDF reads

$$F_{\boldsymbol{X}}(\boldsymbol{x}|\boldsymbol{\theta}) = F_{\mathrm{C}}(F_{X_1}(x_1|\boldsymbol{\theta}_1), F_{X_2}(x_2|\boldsymbol{\theta}_2), \ldots, F_{X_n}(x_n|\boldsymbol{\theta}_n)|\boldsymbol{\theta}_{\mathrm{C}}) \tag{28}$$

For the marginal distributions, our working assumption is that only the mean value and standard deviation, μ_i, σ_i, are given for each random variable. This information is only sufficient for a Gaussian random variable but insufficient for distributions which are skewed or which have more than two parameters. The Beta distribution provides the flexibility to fix the mean value and standard deviation and, at the same time to model a skewness or other higher-order moment information. The uniform distribution is obtained as a special case and even the normal distribution can be approximated with high accuracy on a bounded domain through a suitable choice of the distribution parameters. Hence, every random variable is assumed here to be Beta-distributed $X_i \sim \mathcal{B}(a_i, b_i, \alpha_i, \beta_i)$, where $[a_i, b_i]$ represents the support of the distribution and α_i, β_i are shape parameters. The density on $[0,1]$ is given as $f_{X_i} = x^{\alpha_i - 1}(1-x)^{\beta_i - 1}/B(\alpha_i, \beta_i)$, where B denotes the Beta function; an arbitrary support can be handled with a change of variables. The parameters a_i, b_i are chosen such that mean value and standard deviation match, whereas $\boldsymbol{\theta}_i = (\alpha_i, \beta_i)^\top$ are unknown and simply assumed to lie in some interval. A p-box originating from interval-valued distribution parameters is called a distributional p-box.

For the dependence model, a Gaussian copula is employed

$$F_{\mathrm{C}}(u_1, \ldots, u_n) = \Phi_{\boldsymbol{R}}(\Phi^{-1}(u_1), \ldots, \Phi^{-1}(u_n)), \tag{29}$$

where Φ^{-1} denotes the inverse CDF of a standard Gaussian random variable and $\Phi_{\boldsymbol{R}}$ the CDF of a multivariate mean-free Gaussian vector with correlation matrix $\boldsymbol{R} \in \{-1, 1\}^{n \times n}$. If all off-diagonal elements of $\boldsymbol{R}$ are zero, then all random variables are independent. Hence, dependence between the variables can be introduced through the correlation matrix $\boldsymbol{R}$. In particular, if two random variables are dependent, but the precise functional relationship is unknown, we introduce an entry $r_{ij} \in [-1, 1]$ in $\boldsymbol{R}$. Furthermore, all diagonal entries are set to one. The p-box parameters are hence, all n_{C} non-zero off-diagonal entries as $\boldsymbol{\theta}_{\mathrm{C}} = \{r_{ij} \neq 0\}$ with the restriction that the matrix remains non-negative definite. It should be noted that a common alternative to assuming intervals for $\boldsymbol{\theta}$ and $\boldsymbol{\theta}_{\mathrm{C}}$ consists of posing a (prior) distribution over the sets D_{C} and D_n, which results again in a Bayesian probabilistic treatment of epistemic uncertainties [68].

In analogy to the standard probabilistic setting, where the input distribution needs to be propagated to the model output, the input p-boxes need to be propagated as well. Various algorithms such as an interval Monte Carlo method [74] and polynomial chaos techniques [69] can be used to this end. However, these algorithms typically assume the independence of the model inputs, and it is unclear how to combine them with imprecise copulas.

To include dependence, one can proceed by drawing $\boldsymbol{U}^{(k)}$, for $k = 1, \ldots, I$, which consists of independent uniformly distributed random variables in $[0, 1]$. Then, define

$$\boldsymbol{U}^{(k)} \mapsto \boldsymbol{V} = (\Phi^{-1}(U_1^{(k)}), \ldots, \Phi^{-1}(U_n^{(k)}))^{\top} \tag{30a}$$

$$\boldsymbol{V} \mapsto \boldsymbol{W}_{\boldsymbol{\theta}_{\mathrm{C}}} = \boldsymbol{L}_{\boldsymbol{\theta}_{\mathrm{C}}} \boldsymbol{V} \tag{30b}$$

where $\boldsymbol{L}\boldsymbol{L}^{\top} = \boldsymbol{R}$. Equations (30) represent the NATAF transformation, see for instance [71] and the references therein, with copula parameters entering through the Cholesky factor $\boldsymbol{L} = \boldsymbol{L}_{\boldsymbol{\theta}_{\mathrm{C}}}$. We can then obtain a box in the input domain as

$$\underline{x}_i^{(k)} = \min_{\boldsymbol{\theta}_{\mathrm{C}}} \overline{F}_{X_i}^{-1}(\Phi((\boldsymbol{W}_{\boldsymbol{\theta}_{\mathrm{C}}})_i)), \qquad \overline{x}_i^{(k)} = \max_{\boldsymbol{\theta}_{\mathrm{C}}} \underline{F}_{X_i}^{-1}(\Phi((\boldsymbol{W}_{\boldsymbol{\theta}_{\mathrm{C}}})_i))$$

Finally, we maximize (minimize) over the resulting input domains

$$D_n^{(k)} = [\underline{x}_1^{(k)}, \overline{x}_1^{(k)}] \times \cdots \times [\underline{x}_n^{(k)}, \overline{x}_n^{(k)}], \tag{31}$$

to obtain the output intervals

$$\underline{y}^{(k)} = \min_{\boldsymbol{x} \in D_n^{(k)}} \mathcal{M}(\boldsymbol{x}), \quad \overline{y}^{(k)} = \max_{\boldsymbol{x} \in D_n^{(k)}} \mathcal{M}(\boldsymbol{x}) \tag{32}$$

The output p-box is obtained by constructing empirical CDFs from $\{\underline{y}^{(k)}\}_{k=1}^{K}$ and $\{\overline{y}^{(k)}\}_{k=1}^{K}$, respectively, where each data point has equal weight. In the numerical results section, p-boxes are propagated through a PC surrogate model instead of the original noise model $\mathcal{M}$. This step introduces an additional approximation, which needs to be controlled carefully together with the sampling error.

Appendix B: Additional Numerical Results

This appendix shows additional numerical results for the departure scenario, namely: Figure 11 which complements Figure 3, Figure 12 which complements Figure 4, and Figure 13 which complements Figure 5.

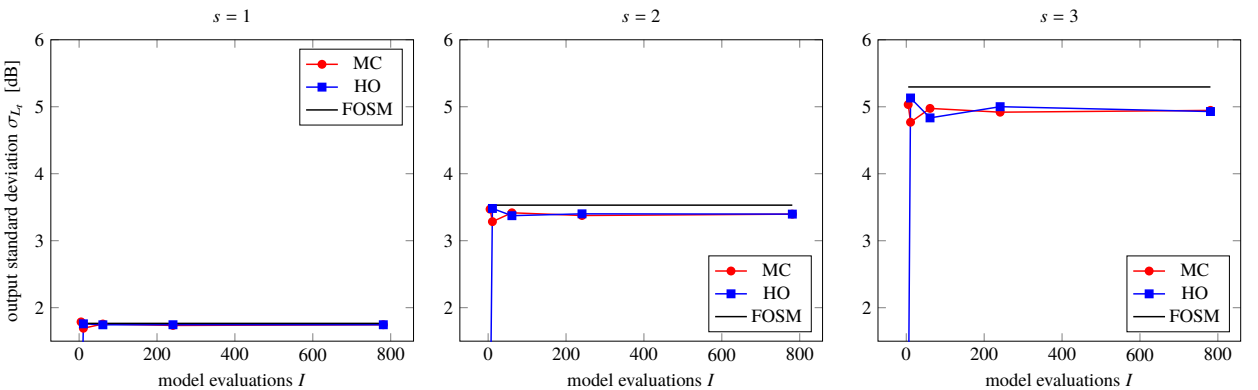

Fig. 11 Comparison of computed standard deviations with FOSM, higher-order (HO), and Monte Carlo method (MC) for $s = 1, 2, 3$ and the departure scenario.

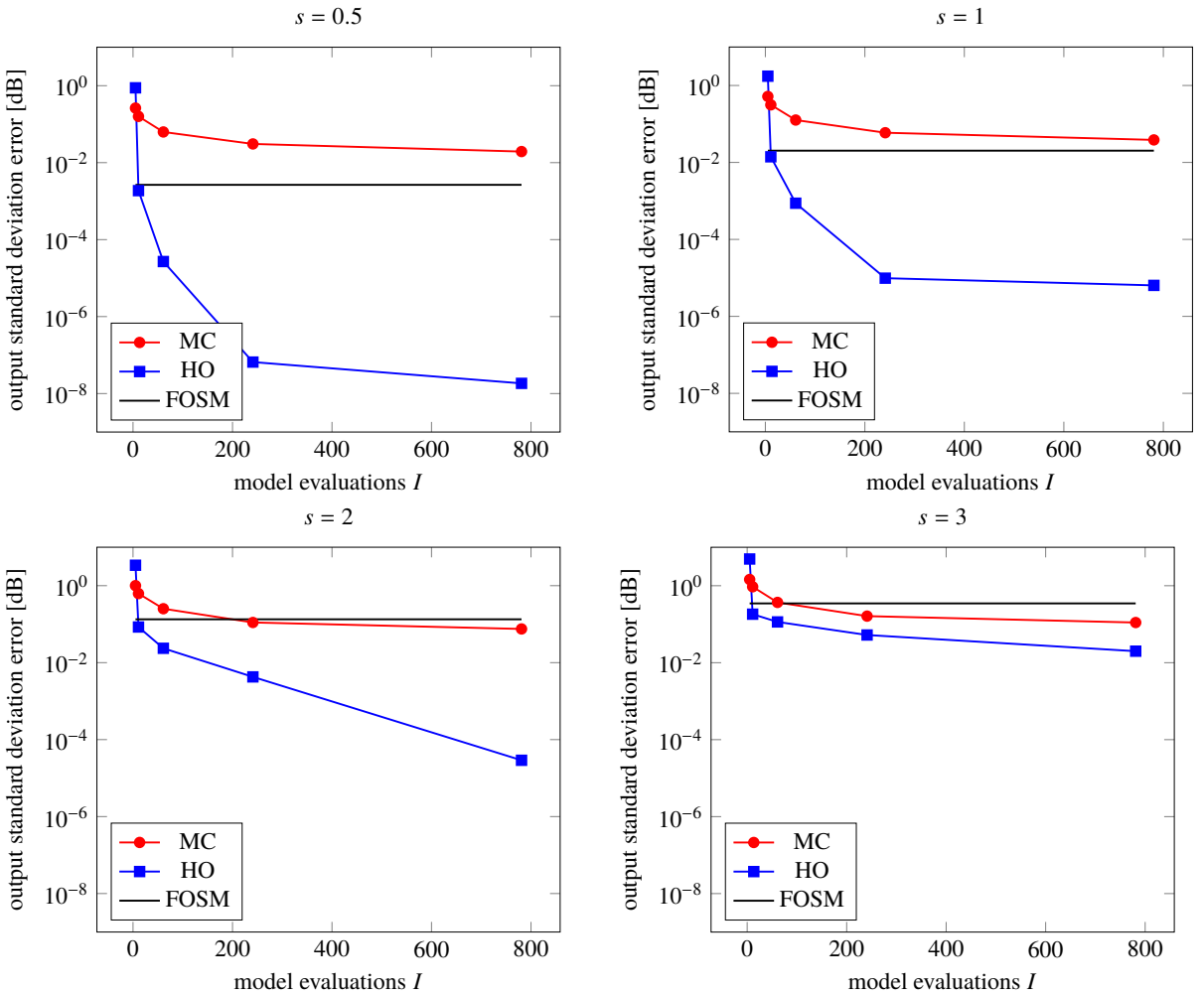

Fig. 12 Comparison of computed standard deviation and errors with FOSM, higher-order (HO), and Monte Carlo (MC) for $s = 0.5, 1, 2, 3$ and the departure scenario. The errors are computed with respect to a quadrature rule with an accuracy of ten digits.

References

[1] Najm, H. N., "Uncertainty Quantification and Polynomial Chaos Techniques in Computational Fluid Dynamics," *Annual Review of Fluid Mechanics*, Vol. 41, 2008, pp. 35–52. doi:10.1146/annurev.fluid.010908.165248.

[2] Ghanem, R., and Spanos, P., *Stochastic Finite Elements: A Spectral Approach*, Springer Verlag, 1991. doi:10.1007/978-1-4612-3094-6.

[3] Thapa, M., Mulani, S. B., and Walters, R. W., *Uncertainty Quantification: Advances in Research and Applications*, Nova Publishers, 2019, Chaps. Polynomial Chaos for Uncertainty Quantification: Past, Present, and Future, pp. 1–134.

[4] Hammersley, J. M., and Handscomb, D. C., *Monte Carlo Methods*, Methuen's Monographs on Applied Probability and Statistics, 1964. doi:10.1007/978-94-009-5819-7.

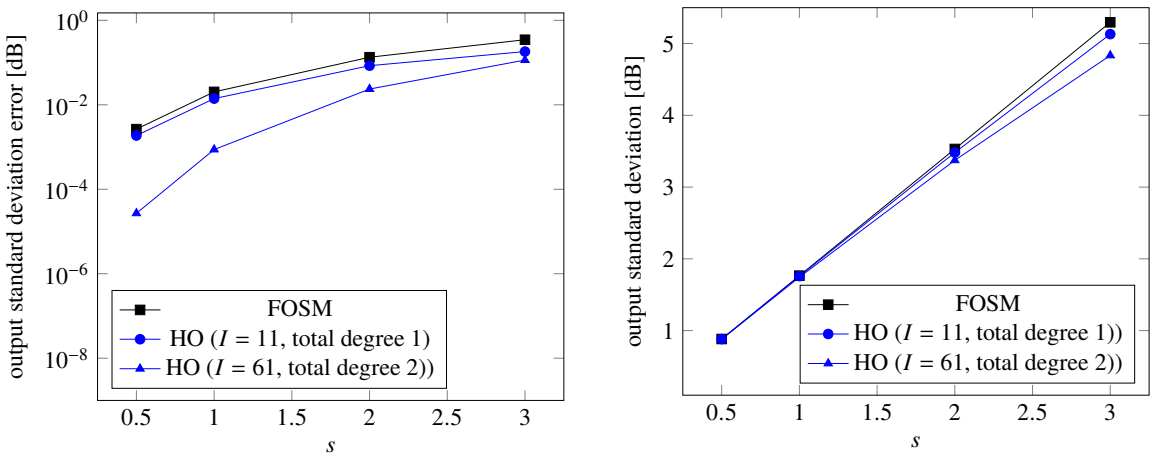

Fig. 13 Approximation of standard deviation errors (left) and standard deviations (right) of output uncertainties for FOSM and higher-order (HO) approach with variable number of model evaluations and uncertainty sizes s for the departure scenario.

[5] Liu, W. K., Belytschko, T., and Mani, A., "Probabilistic Finite Elements for Nonlinear Structural Dynamics," *Computer Methods in Applied Mechanics and Engineering*, Vol. 56, No. 1, 1986, pp. 61–81. doi:10.1016/0045-7825(86)90136-2.

[6] Matthies, H. G., Brenner, C. E., Bucher, C. G., and Soares, C. G., "Uncertainties in Probabilistic Numerical Analysis of Structures and Solids-Stochastic Finite Elements," *Structural Safety*, Vol. 19, No. 3, 1998, pp. 283–336. doi:10.1016/s0167-4730(97)00013-1.

[7] Deodatis, G., and Shinozuka, M., "The Weighted Integral Method, II: Response Variability and Reliability," *Journal of Engineering Mechanics*, Vol. 117, No. 8, 1991, pp. 1865–1877. doi:10.1061/(asce)0733-9399(1991)117:8(1865).

[8] Ditlevsen, O., and Madsen, H. O., *Structural Reliability Methods*, Chichester: Wiley, 1996.

[9] Wiener, N., "The Homogenous Chaos," *American Journal of Mathematics*, Vol. 60, No. 4, 1938, pp. 897—-936.

[10] Cameron, R. H., and Martin, W. T., "The Orthogonal Development of Non-Linear Functionals in Series of Fourier-Hermite Functionals," *Annals of Mathematics*, Vol. 48, No. 2, 1947, pp. 385–392.

[11] Xiu, D., and Karniadakis, G. E., "Modeling Uncertainty in Flow Simulations via Generalized Polynomial Chaos," *Journal of Computational Physics*, Vol. 187, No. 1, 2003, pp. 137–167. doi:10.1016/S0021-9991(03)00092-5.

[12] Mathelin, L., Hussaini, M. Y., and Zang, T. A., "Stochastic Approaches to Uncertainty Quantification in CFD Simulations," *Numerical Algorithms*, Vol. 38, No. 1, 2005, pp. 209–236. doi:10.1007/bf02810624.

[13] Hosder, S., Walters, R. W., and Balch, M., "Point-Collocation Nonintrusive Polynomial Chaos Method for Stochastic Computational Fluid Dynamics," *AIAA Journal*, Vol. 48, No. 12, 2010, pp. 2721–2730. doi:10.2514/1.39389.

[14] Thapa, M., Mulani, S. B., and Walters, R. W., "Stochastic Multi-Scale Modeling of Carbon Fiber Reinforced Composite Laminates with Polynomial Chaos Expansion," *Composite Structures*, Vol. 213, 2019, pp. 82–97. doi:10.1016/j.compstruct.2019.01.068.

[15] Hover, F. S., and Triantafyllou, M. S., "Application of Polynomial Chaos in Stability and Control," *Automatica*, Vol. 42, No. 5, 2006, pp. 789–795. doi:10.1016/j.automatica.2006.01.010.

[16] Bertsch, L., Clark, I., Thomas, R., Sanders, L., and LeGriffon, I., "The Aircraft Noise Simulation Working Group (ANSWr) - Tool Benchmark and Reference Aircraft Results," *25th AIAA/CEAS Aeroacoustics Conference*, AIAA, Delft, The Netherlands, 2019, pp. 1–19. doi:10.2514/6.2019-2539.

[17] Sanders, L., Thomas, R., Bertsch, L., LeGriffon, I., Clark, I., June, J., and Lorteau, M., "The Aircraft Noise Simulation Working Group (ANSWr) – V-2 Aircraft Results," *25th AIAA/CEAS Aeroacoustics Conference*, AIAA, Delft, The Netherlands, 2019, pp. 1–18. doi:10.2514/6.2019-2540.

[18] Bertsch, L., Schäfer, B., and Guerin, S., "Uncertainty Analysis for Parametric Aircraft System Noise Prediction," *Journal of Aircraft*, Vol. 56, No. 2, 2019, pp. 529–544. doi:10.1007/s13272-019-00374-5.

[19] Thomann, G., "Uncertainties of Measured and Calculated Aircraft Noise and Consequences in Relation to Noise Limits," Tech. Rep. PhD Thesis ETH Zürich, No. 17433, ETH, Zürich, 2007.

[20] Schäffer, B., Plüss, S., and Thomann, G., "Estimating the Model-Specific Uncertainty of Aircraft Noise Calculations," *Applied Acoustics*, Vol. 84, No. 1, 2014, pp. 58–72. doi:10.1016/j.apacoust.2014.01.009.

[21] Burley, C., Rawls, J., Berton, J., and Marcolini, M., "Assessment of NASA's Aircraft Noise Prediction Capabilities - Chapter 2: Aircraft System Noise Prediction," Tech. Rep. NASA Technical Report, NASA/TP-2012-215653, NASA, Langley, Virgina, USA, 2012.

[22] Der Bundesminister für Umwelt Naturschutz und Reaktorsicherheit, "Bekanntmachung der Anleitung zur Datenerfassung über den Flugbetrieb (AzD) und der Anleitung zur Berechnung von Lärmschutzbereichen (AzB) vom 19. November 2008," BAnz. Nr. 195a vom 23. Dezember 2008, S. 1-232, Dec. 2008.

[23] Isermann, U., and Vogelsang, B., "AzB and ECAC Doc.29 - Two Best-Practice European Aircraft Noise Prediction Models," *Noise Control Engineering Journal*, Vol. 58, No. 4, 2010, pp. 455–461. doi:10.3397/1.3455442.

[24] Empa, "FLULA 2, Ein Verfahren zur Berechnung und Darstellung der Fluglärmbelästigung," Tech. Rep. Programm Dokumentation, Version 4, Eidgenössische Materialprüefungs- und Forschungsanstalt (Empa), 2010. Http://www.empa.ch/web/s509/flula2.

[25] European Civil Aviation Conference (ECAC), "Methodology for Computing Noise Contours around Civil Airports. Volume 1: Applications Guide, Volume 2: Technical Guide, Volume 3: Part 1 - Reference cases and verification framework," Tech. Rep. ECAC.CEAC Doc.29, 4rd Edition, ECAC, 4, December 2016. Https://www.ecac-ceac.org/ecac-docs.

[26] International Civil Aviation Organization (ICAO), "Recommended Method for Computing Noise Contours Around Airports," Tech. Rep. ICAO Doc.9911, 1st edition, ICAO, 2008.

[27] Bertsch, L., Simons, D., and Snellen, M., "Aircraft Noise: The Major Sources, Modelling Capabilities, and Reduction Possibilities," Tech. Rep. DLR IB 224-2015 A 110, Deutsches Zentrum für Luft- und Raumfahrt (DLR), 2015. Internal report.

[28] Isermann, U., and Bertsch, L., "Aircraft Noise Immission Modeling," *CEAS Aeronautical Journal*, Vol. 10, No. 1, 2019, pp. 287–311. doi:10.1007/s13272-019-00374-5, in Special Issue: Aircraft Noise Generation and Assessment.

[29] Lopes, L., and Burley, C., "Design of the Next Generation Aircraft Noise Prediction Program: ANOPP2," *32th AIAA Aeroacoustics Conference*, AIAA, Portland, Oregon, USA, 2011, pp. 1–21. doi:10.2514/6.2011-2854.

[30] Malbéqui, P., Rozenberg, Y., and Bulté, J., "Aircraft Noise Modelling and Assessment in the IESTA Program," *InterNoise*, AIAA, Osaka, Japan, 2011, pp. 1–21.

[31] Bertsch, L., Guerin, S., and Dobrzynski, W., "Tool Development for Low-Noise Aircraft Design," *Journal of Aircraft*, Vol. 47(2), 2010, pp. 694–699. doi:10.2514/1.43188.

[32] Dobrzynski, W., Chow, L., Guion, P., and Shiells, D., "A European Study on Landing Gear Airframe Noise Sources," *6th AIAA/CEAS Aeroacoustics Conference*, AIAA, Lahaina, Hawaii/USA, 2000, pp. 1–15. doi:10.2514/6.2000-1971.

[33] Dobrzynski, W., and Pott-Pollenske, M., "Slat Noise Source Studies for Farfield Noise Prediction," *7th AIAA/CEAS Aeroacoustics Conference*, AIAA, Maastricht, Netherlands, 2001, pp. 1–17. doi:10.2514/6.2001-2158.

[34] Pott-Pollenske, M., Dobrzynski, W., Buchholz, H., Gehlhar, B., and Walle, F., "Validation of Semiempirical Airframe Noise Prediction Method through Dedicated A319 Flyover Noise Measurements," *8th AIAA/CEAS Aeroacoustics Conference*, AIAA, Breckenridge, Colorado, 2002, pp. 1–19. doi:10.2514/6.2002-2470.

[35] Bertsch, L., "Noise Prediction Within Conceptual Aircraft Design," Tech. Rep. DLR-FB-2013-20, DLR, Deutsches Zentrum für Luft- und Raumfahrt (DLR), Göttingen, 2013.

[36] Rossignol, K.-S., "Development of an Empirical Prediction Model for Flap Side-Edge Noise," *16th AIAA/CEAS Aeroacoustics Conference*, AIAA, Stockholm, Sweden, 2010, pp. 1–19. doi:10.2514/6.2010-3836.

[37] Rossignol, K.-S., "Empirical Prediction of Airfoil Tip Noise," *17th AIAA/CEAS Aeroacoustics Conference*, AIAA, Portland, Oregon, USA, 2011, pp. 1–18. doi:10.2514/6.2011-2733.

[38] Heidmann, M., "Interim Prediction Method for Fan and Compressor Source Noise," Tech. Rep. NASA TMX-71763, NASA, NASA, 1979.

[39] Moreau, A., Guérin, S., and Busse, S., "A Method Based on the Ray Structure of Acoustic Modes for Predicting the Liner Performance in Annular Ducts with Flow," *NAG/DAGA International Conference on Acoustics*, NAG/DAGA, Rotterdam, Netherlands, 2009, pp. 1–17.

[40] Stone, J., Groesbeck, D., and Zola, C., "Conventional Profile Coaxial Jet Noise Prediction," *AIAA Journal*, Vol. 21(1), 1983, pp. 336–342. doi:10.2514/3.8077.

[41] International Organization for Standardization (ISO), "Acoustics - Attenuation of Sound during Propagation Outdoors. Part 1: Calculation of the Absorption of Sound by the Atmosphere," Tech. Rep. ISO 9613-1:1993, ISO, June 1993.

[42] SAE International, "Prediction Method for Lateral Attenuation of Airplane Noise during Takeoff and Landing," Tech. Rep. SAE AIR 1751, SAE, 1991.

[43] Zein, S., Colson, B., and Glineur, F., "An Efficient Sampling Method for Regression-Based Polynomial Chaos Expansion," *Communications in Computational Physics*, 2013. doi:10.4208/cicp.020911.200412a.

[44] Ray, J., Kieweg, S., Dinzi, D., Carnes, B., Weirs, V. G., Freno, B., Howard, M., Smith, T., Nompelis, I., and Candler, G. V., "Estimation of Inflow Uncertainties in Laminar Hypersonic Double-Cone Experiments," *AIAA Journal*, Vol. 58, 2020, pp. 4461–4474. doi:10.2514/1.j059033.

[45] Clark Jr., D. L., Bae, H., and Forster, E. E., "Gaussian Surrogate Dimension Reduction for Efficient Reliability-Based Design Optimization," *AIAA Journal*, Vol. 58, 2020, pp. 1–15. doi:10.2514/1.j059325.

[46] Rumpfkeil, M. P., and Beran, P. S., "Multifidelity Sparse Polynomial Chaos Surrogate Models Applied to Flutter Databases," *AIAA Journal*, Vol. 58, 2019, pp. 1292–1303. doi:10.2514/1.j058452.

[47] Zhou, Y., and Lu, Z., "Active Polynomial Chaos Expansion for Reliability-Based Design Optimization," *AIAA Journal*, Vol. 57, 2019, pp. 5431–5446. doi:10.2514/1.j058020.

[48] Weinmeister, J., Gao, X., and Roy, S., "Analysis of a Polynomial Chaos-Kriging Metamodel for Uncertainty Quantification in Aerodynamics," *AIAA Journal*, Vol. 57, 2019, pp. 2280–2296. doi:10.2514/1.j057527.

[49] Rumpfkeil, M. P., and Beran, P. S., "Multi-Fidelity, Gradient-enhanced, and Locally Optimized Sparse Polynomial Chaos and Kriging Surrogate Models Applied to Benchmark Problems," *AIAA Scitech 2020 Forum*, Orlando, Florida, USA, 2020, pp. 1–18. doi:10.2514/6.2020-0677.

[50] Devathi, H., Hu, Z., and Mahadevan, S., "Snap-Through Buckling Reliability Analysis Under Spatiotemporal Variability and Epistemic Uncertainty," *AIAA Journal*, Vol. 54, 2016, pp. 3981–3993. doi:10.2514/1.j054920.

[51] Mishra, A. A., Mukhopadhaya, J., Iaccarino, G., and Alonso, J., "Uncertainty Estimation Module for Turbulence Model Predictions in SU2," *AIAA Journal*, Vol. 57, 2018, pp. 1066–1077. doi:10.2514/1.j057187.

[52] Kadyk, T., Schenkendorf, R., Hawner, S., Yildiz, B., and Römer, U., "Design of fuel cell systems for aviation: representative mission profiles and sensitivity analyses," *Frontiers in Energy Research*, Vol. 7, 2019, p. 35. doi:10.3389/fenrg.2019.00035.

[53] Guruprasad, S. M., Ram, P. R. M., Blech, C., Römer, U., and Langer, S. C., "Aircraft Cabin Noise Prediction Under Uncertainty," *Fundamentals of High Lift for Future Civil Aircraft*, Springer, 2021, pp. 247–261. doi:10.1007/978-3-030-52429-6_16.

[54] Römer, U., Zafar, S. A., and Fezans, N., "A Multifidelity Approach for Uncertainty Propagation in Flight Dynamics," *Fundamentals of High Lift for Future Civil Aircraft*, Springer, 2021, pp. 463–478. doi:10.1007/978-3-030-52429-6_28.

[55] West IV, T. K., Reuter, B. W., Walker, E. L., Kleb, B., and Park, M. A., "Uncertainty Quantification and Certification Prediction of Low-Boom Supersonic Aircraft Configurations," *Journal of Aircraft*, Vol. 54, 2017, pp. 40–53. doi:10.2514/1.c033907.

[56] Kennedy, M. C., and O'Hagan, A., "Bayesian Calibration of Computer Models," *Journal of the Royal Statistical Society: Series B (Statistical Methodology)*, Vol. 63, No. 3, 2001, pp. 425–464. doi:10.1111/1467-9868.00294.

[57] Haldar, A., and Mahadevan, S., *Probability, Reliability, and Statistical Methods in Engineering Design*, J. Wiley & Sons, Inc., 2000.

[58] Trefethen, L. N., "Is Gauss Quadrature Better than Clenshaw–Curtis?" *SIAM Review*, Vol. 50, No. 1, 2008, pp. 67–87. doi:10.1137/060659831.

[59] Narayan, A., and Jakeman, J. D., "Adaptive Leja Sparse Grid Constructions for Stochastic Collocation and High-Dimensional Approximation," *SIAM Journal on Scientific Computing*, Vol. 36, No. 6, 2014, pp. A2952–A2983. doi:10.1137/140966368.

[60] Xiang, S., and Bornemann, F., "On the Convergence Rates of Gauss and Clenshaw–Curtis Quadrature for Functions of limited Regularity," *SIAM Journal on Numerical Analysis*, Vol. 50, No. 5, 2012, pp. 2581–2587. doi:10.1137/120869845.

[61] Debusschere, B. J., Najm, H. N., Pebay, P. P., Knio, O. M., Ghanem, R. G., and Le Maitre, O. P., "Numerical Challenges in the Use of Polynomial Chaos Representations for Stochastic Processes," *SIAM Journal on Scientific Computing*, Vol. 26, No. 2, 2004, pp. 698–719. doi:10.1137/s1064827503427741.

[62] Thapa, M., Mulani, S. B., and Walters, R. W., "A New Non- Intrusive Polynomial Chaos using Higher Order Sensitivities," *Computer Methods in Applied Mechanics and Engineering*, Vol. 328, 2018, pp. 594–611. doi:10.1016/j.cma.2017.09.024.

[63] Bungartz, H. J., and Griebel, M., "Sparse Grids," *Acta Numerica*, Vol. 13, 2004, pp. 1–123. doi:10.1017/S0962492904000182.

[64] Thapa, M., Mulani, S. B., and Walters, R. W., "Adaptive Weighted Least-Squares Polynomial Chaos with Basis Adaptivity and Sequential Adaptive Sampling," *Computer Methods in Applied Mechanics and Engineering*, Vol. 360, 2020, p. 112769. doi:10.1016/j.cma.2019.112759.

[65] Jakeman, J. D., Eldred, M. S., and Sargsyan, K., "Enhancing L1– Minimization Estimates of Polynomial Chaos Expansions Using Basis Selection," *Journal of Computational Physics*, Vol. 289, 2015, pp. 18–34. doi:10.1016/j.jcp.2015.02.025.

[66] Sudret, B., "Global Sensitivity Analysis Using Polynomial Chaos Expansions," *Reliability Engineering & System Safety*, Vol. 93, No. 7, 2008, pp. 964–979. doi:10.1016/j.ress.2007.04.002.

[67] Oberkampf, W. L., Tucker, W. T., Zhang, J., Ginzburg, L., Berleant, D. J., Ferson, S., Hajagos, J., and Nelsen, R. B., "Dependence in Probabilistic Modeling, Dempster-Shafer Theory, and Probability Bounds Analysis." Tech. rep., Sandia National Laboratories, 2004.

[68] Roy, C. J., and Oberkampf, W. L., "A Comprehensive Framework for Verification, Validation, and Uncertainty Quantification in Scientific Computing," *Computer Methods in Applied Mechanics and Engineering*, Vol. 200, No. 25-28, 2011, pp. 2131–2144. doi:10.1016/j.cma.2011.03.016.

[69] Schöbi, R., and Sudret, B., "Uncertainty Propagation of P-Boxes using Sparse Polynomial Chaos Expansions," *Journal of Computational Physics*, Vol. 339, 2017, pp. 307–327. doi:10.1016/j.jcp.2017.03.021.

[70] Jankoski, R., Römer, U., and Schöps, S., "Stochastic Modeling of Magnetic Hysteretic Properties by Using Multivariate Random Fields," *International Journal for Uncertainty Quantification*, Vol. 9, No. 1, 2019. doi:10.1615/Int.J.UncertaintyQuantification.2019025638.

[71] Lebrun, R., and Dutfoy, A., "An Innovating Analysis of the Nataf Transformation From the Copula Viewpoint," *Probabilistic Engineering Mechanics*, Vol. 24, No. 3, 2009, pp. 312–320. doi:10.1016/j.probengmech.2008.08.001.

[72] Torre, E., Marelli, S., Embrechts, P., and Sudret, B., "A General Framework for Data-Driven Uncertainty Quantification under Complex Input Dependencies using Vine Copulas," *Probabilistic Engineering Mechanics*, Vol. 55, 2019, pp. 1–16. doi:10.1016/j.probengmech.2018.08.001.

[73] Faes, M. G., Daub, M., Marelli, S., Patelli, E., and Beer, M., "Engineering analysis with probability boxes: a review on computational methods," *Structural Safety*, Vol. 93, 2021, p. 102092. doi:10.1016/j.strusafe.2021.102092.

[74] Zhang, H., Mullen, R. L., and Muhanna, R. L., "Interval Monte Carlo Methods for Structural Reliability," *Structural Safety*, Vol. 32, No. 3, 2010, pp. 183–190. doi:10.1016/j.strusafe.2010.01.001.

[75] Xiu, D., and Karniadakis, G. E., "The Wiener–Askey Polynomial Chaos for Stochastic Differential Equations," *SIAM Journal on Scientific Computing*, Vol. 24, No. 2, 2002, pp. 619–644. doi:10.1137/S1064827501387826.

[76] Marelli, S., and Sudret, B., "UQLab: A Framework for Uncertainty Quantification in Matlab," *Vulnerability, Uncertainty, and Risk: Quantification, Mitigation, and Management*, ETH Zürich, 2014, pp. 2554–2563.

[77] Sklar, A., "Random Variables, Distribution Functions, and Copulas: A Personal Look Backward and Forward," *Lecture Notes-Monograph Series*, 1996, pp. 1–14.